UDC 621.039.623:533.9.082

HYDROGEN AND HELIUM DISCHARGES IN THE GOLEM TOKAMAK

G.A. Sarancha[1, 2], A.S. Drozd[1, 3], I.A. Emekeev[1, 2], S.A. Ganin[1, 3], D. Kropackova[4], I.S. Kudashev[1, 3], V.V. Kulagin[1, 3], M. Lauerova[4], A.V. Melnikov[1, 2, 3], N.S. Sergeev[1, 3], O.D. Krokhalev[1, 2], J. Stockel[4], V. Svoboda[4]

[1]*National Research Center «Kurchatov Institute», Moscow, Russia*
[2]*Moscow Institute of Physics and Technology (National Research University), Dolgoprudny, Russia*
[3]*National Research Nuclear University MEPhI, Moscow, Russia*
[4]*Faculty of Nuclear Sciences and Physical Engineering, Czech Technical University in Prague, Czech Republic*

The helium plasma properties and confinement remain an important area of research in modern fusion devices. This work is dedicated to the helium plasma initiation and control in a small-scale tokamak GOLEM compared to hydrogen plasma. Helium and hydrogen plasmas are comprehensively compared and the optimum operational conditions for the start-up are found. Long-range correlations between low-frequency (<50 kHz) electrostatic and magnetic oscillations are found, as well as broadband (<250 kHz) magnetic oscillations resolved in frequency and wave vector in helium plasma.

Key words: GOLEM tokamak, comparison of plasma discharges in hydrogen and helium, low-frequency electrostatic and magnetic oscillations.

DOI: 10.21517/0202-3822-2021-44-4-92-110

РАЗРЯДЫ В ВОДОРОДНОЙ И ГЕЛИЕВОЙ ПЛАЗМЕ ТОКАМАКА GOLEM

Г.А. Саранча[1, 2], А.С. Дрозд[1, 3], И.А. Емекеев[1, 2], С.А. Ганин[1, 3], Д. Кропачкова[4], И.С. Кудашев[1, 3], В.В. Кулагин[1, 3], М. Лауэрова[4], А.В. Мельников[1, 2, 3], Н.С. Сергеев[1, 3], О.Д. Крохалев[1, 2], Я. Штокель[4], В. Свобода[4]

[1]*Национальный исследовательский центр «Курчатовский институт», Москва, Россия*
[2]*Московский физико-технический институт (Национальный исследовательский университет), Долгопрудный, Россия*
[3]*Национальный исследовательский ядерный университет «МИФИ», Москва, Россия*
[4]*Факультет ядерных наук и физической инженерии, Чешский технический университет в Праге, Чешская Республика*

Свойства гелиевой плазмы и её удержание остаются важными темами исследований в современных термоядерных установках. Эта работа посвящена сравнению создания гелиевой и водородной плазмы и управлению ими в небольшом токамаке GOLEM. Проведено всестороннее сравнение гелиевой и водородной плазмы и найдены оптимальные рабочие условия для их получения. Обнаружены дальнодействующие зависимости корреляции между низкочастотными (<50 кГц) электростатическими и магнитными колебаниями, а также широкополосными (<250 кГц) магнитными колебаниями, разрешёнными по частоте и волновому вектору в гелиевой плазме.

Ключевые слова: токамак GOLEM, сравнение разрядов в водородной и гелиевой плазме, низкочастотные электростатические и магнитные колебания.

INTRODUCTION

Experiments with helium plasma are quite unique in modern fusion devices. They are mostly made on large scale devices and dedicated to ITER relevant studies for non-nuclear phase of operation. The performance of plasma discharges in helium is always lower than that in hydrogen or deuterium with identical plasma current I_{pl}, toroidal magnetic field B_{t}, line-averaged electron density $\bar{n}_e$ and heating power [1]. It was shown that energy confinement time for helium plasmas is about 30% lower than for deuterium ones, contradicting to gyro-Bohm scaling. It might be coupled to the isotope effect, which suggests better confinement for the isotope with larger mass. Several theoretical mechanisms including $\mathbf{E}\times\mathbf{B}$ shearing [2, 3] and collisional effects [4] were proposed to explain this effect but there is no satisfactory explanation so far.

To expand the knowledge of helium plasma confinement parameters, it will be helpful to investigate the operational domain from large machines to small-scale ones with low electron temperature and plasma density.

Small and medium-size fusion devices could be of a great support for the mainstream plasma research in various topics [5—7]. Such research activities are coordinated by IAEA Coordinated Research Projects (CRP) with participation of the GOLEM tokamak [8], formerly called CASTOR [9, 10]. In addition to the research tasks the teaching and the training of the young plasma physicists becomes an essential element of the CRP [11].

The experiments aimed at learning the basics of helium plasma confinement were performed remotely in GOLEM by a team of master students of National Research Nuclear University MEPhI and National Research University MIPT as a part of the course «Technology of the thermonuclear experiment».

Special attention is paid to the gas breakdown process and its comparison for hydrogen and helium discharges. For this study, a series of discharges with vacuum vessel pre-cleaning have been produced. Hydrogen and helium plasmas were studied with identical pre-selected discharge setup parameters allowing the detailed comparison.

In addition, the study is focused on the electrostatic and magnetic turbulence and their correlation properties. Long-range correlations are characteristic features of Zonal Flows — a mechanism of the broadband turbulence self-regulations, 12]. Zonal Flows and their higher frequency counterpart Geodesic Acoustic Modes were recently studied in tokamaks [13—15] and stellarators [16—19] of small and medium size. The search for Zonal Flows in the GOLEM tokamak could be one of the most important contributions to the mainstream fusion research.

THE GOLEM TOKAMAK

The GOLEM tokamak [20] has a circular cross section with the major/minor radius $R = 0.4$ m, $a = 0.1$ m [21]. After upgrades the circular stainless-steel vessel was equipped with a molybdenum poloidal limiter located at radius $a_{lim} = 0.085$ m. Due to the origin of the machine whole vacuum chamber is surrounded by a copper shell. The power supply system is based on capacitor banks. Each of the individual winding, including central solenoid, is connected to separated capacitor banks, which allows to easily adjust the desired value of current passing through the coils. GOLEM has a unique capability of the remote control via Internet [22].

Prior to the plasma experiment, the vacuum vessel was carefully conditioned by inductive heating at up to 200 °C for 60 min, which was followed by a cleaning glow discharge in order to remove impurities from the vacuum vessel. Glow discharge cleaning had a gas pressure around 1 Pa, duration 20 min., a discharge current of about 0.5 A, and working gas hydrogen for H-plasmas and helium for He-plasmas. Such treatment results in a background gas pressure as low as 0.1 mPa.

The GOLEM gas control system has no option for active gas puffing during the shot, so the experimental data discussed here are performed in ohmic discharges with no density control. That is why typical values of electron concentration and central electron temperature are about $\bar{n}_e \sim 10^{19}$ m^{-3} and $T_e(0) \sim 100$ eV. For easy plasma start-up, in view of the difference in ionization energy for hydrogen and helium gases, conventional pre-ionization by an electron gun was used.

DIAGNOSTICS ON GOLEM

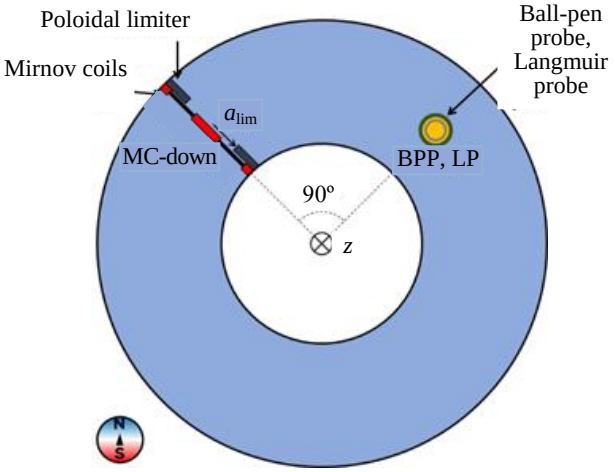

Fig. 1. Diagnostic set-up. View of the GOLEM tokamak from the bottom

The machine is equipped with set of standard diagnostics [23], which are capable to measure the loop voltage U_{loop}, plasma current I_{pl}, toroidal magnetic field B_t and visible light emission. For the studies of magnetic oscillations, GOLEM is equipped with four Mirnov Coils (MC). Electric probes were used to study the edge plasma parameters. In fig. 1 the location of magnetic and electric probes is shown.

Mirnov Coils. For plasma position measurement in GOLEM Mirnov Coils are used. They are placed inside the vacuum chamber at the radius $b = 0.093$ m as shown in fig. 2.

The effective area of each MC is $A = 3.8 \cdot 10^{-3}$ m^2. Coils MC-out and MC-in are used to determine the horizontal plasma position and MC-up and MC-down — to determine the vertical plasma position.

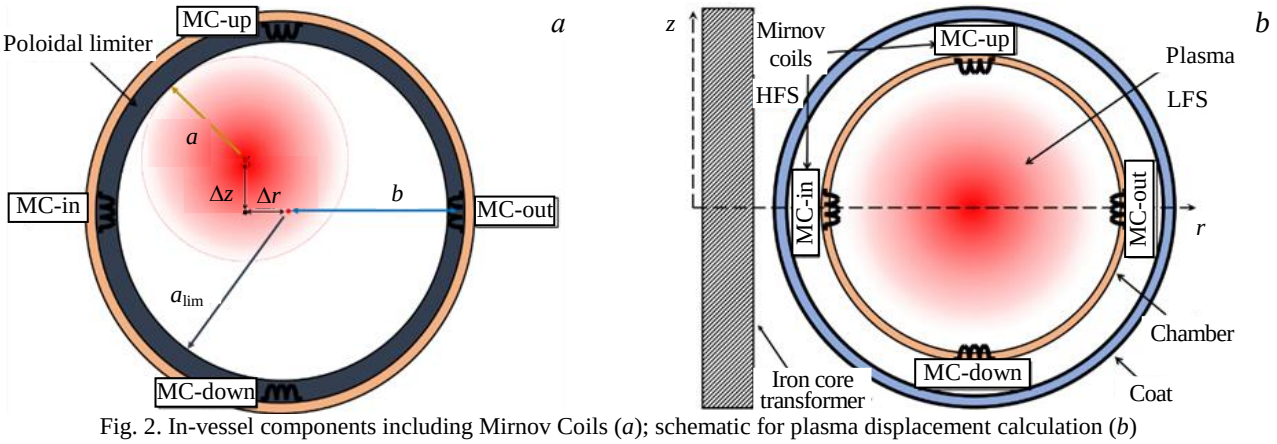

Fig. 2. In-vessel components including Mirnov Coils (*a*); schematic for plasma displacement calculation (*b*)

The coils measure voltage induced by changes in poloidal magnetic field. To get the absolute value of poloidal magnetic field, one should integrate the measured voltage U and normalize by an effective area:

$$B(t) = -\frac{1}{A}\int_0^t U(\tau)\mathrm{d}\tau \quad [\mathrm{T, m^2, V, s}]. \tag{1}$$

Ideally, the axis of the coil is perpendicular to the toroidal magnetic field, but in fact they are slightly deflected, and hence the measured signal is contaminated by some amount of toroidal magnetic field. For the determination of plasma position this parasitic signal should be removed. Vacuum discharge with the same parameters of current drive voltage and toroidal magnetic field as plasma discharge, but without plasma, is used for this purpose. Mirnov coils signal in the vacuum discharge has no plasma signal, but only toroidal magnetic field and also some other magnetic fields e.g. generated by poloidal windings. Such a signal registered during vacuum discharge is subtracted from the active signal from discharge with plasma.

With values of poloidal field on the two opposite sides of the column, plasmas column horizontal displacement [24] can be expressed as:

$$\Delta r = \frac{B_{\text{MC-out}} - B_{\text{MC-in}}}{B_{\text{MC-out}} + B_{\text{MC-in}}} b \quad [\mathrm{m, T}], \tag{2}$$

and for vertical plasma displacement:

$$\Delta z = \frac{B_{\text{MC-up}} - B_{\text{MC-down}}}{B_{\text{MC-up}} + B_{\text{MC-down}}} b \quad [\mathrm{m, T}]. \tag{3}$$

As plasma column is limited by poloidal limiter, for displaced plasma the minor radius a can be calculated as:

$$a = a_{\text{lim}} - \sqrt{\Delta r^2 + \Delta z^2} \quad [\mathrm{m}] \tag{4}$$

(see fig. 2, *b*).

Electric probes. The edge plasma parameters are measured by the combined probe head inserted in the GOLEM vessel through the bottom diagnostic port. The probe head is composed of the Ball Pen Probe (BPP) and the single Langmuir Probe located at the same magnetic surface r_{probe} = 0.085 m, equal to a_{lim}. Both probes operate in the floating regime, their signals are recorded via a voltage divider 1:100 with the total resistivity 0.7 MΩ. BPP directly measures the plasma potential φ_{pl}, as it was shown in [25], and references inside. The Langmuir probe measures the floating potential φ_{fl} (fig. 3).

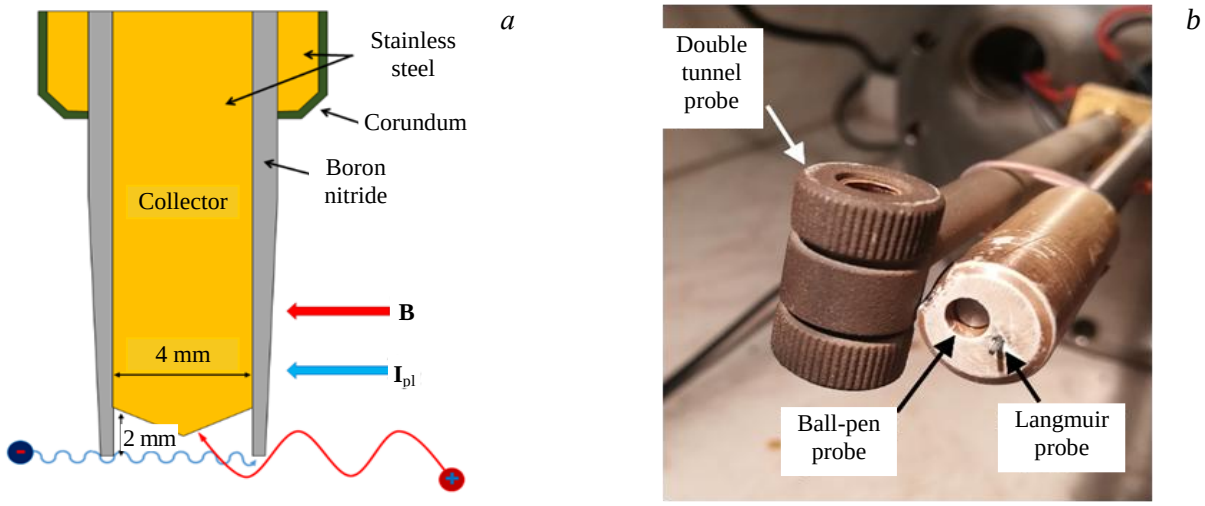

Fig. 3. Electric probes. Schematic and principle of the Ball Pen probe. The collector is located inside an insulated cylinder by the depth of 2 mm. In this case, the collected electron current is significantly screened because of the smaller electron Larmor radius (*a*). Photo of the combined probe head (*b*)

This combined probe head allows determination of the electron temperature by using the expression [26]:

$$T_e = \frac{\varphi_{\text{pl}} - \varphi_{\text{fl}}}{\alpha} \quad [\mathrm{eV, V}]. \tag{5}$$

The calibration factor α is equal to 2.5 V/eV for hydrogen plasmas and 2 V/eV for helium plasmas for typical toroidal magnetic fields of GOLEM. Note that the combined BPP + LP probe head allows T_e measurement with the temporal resolution limited just by the sampling rate of the data acquisition system, which is 1 MSPS.

EXPERIMENTAL SETUP

The present study was performed remotely in May 2020 with 93 discharges in hydrogen and helium executed during two afternoon experimental sessions:

— 53 discharges with helium plasmas — (№ 33 011—33 063);

— 42 discharges with hydrogen plasmas — (№ 33 064—33 105).

Experimental data are stored in the GOLEM database and freely available at http://GOLEM.fjfi.cvut.cz/shots/SHOT#/.

Machine operation was performed in so-called «basic mode», when only two capacitor banks were remotely controlled: the first one for the toroidal field coils (U_{B_t}), and the second one for primary winding of the iron core transformer (U_{CD}) which provides current drive. The working gas (either hydrogen or helium) and its pressure is preselected. The range of the preset control parameters is presented in tab. 1.

T a b l e 1. **Preset parameters of discharges**

Working gas	U_{B_t}, V	B_t, T	U_{CD}, V	τ(U_{CD}), ms	P, mPa	Pre-ionization by electron gun
H/He	1000	0.2—0.3	400 (He)/500 (H)—750	1	10—230	ON

Discharge scenarios for hydrogen and helium plasmas are shown in fig. 4. The data acquisition system collecting all discharge parameters starts at t = 0. The toroidal magnetic field starts at t = 1 ms and increases in time. After the delay τ_{CD} = 1 ms, the capacitor bank for powering the primary winding of the transformer is switched on and generates the loop voltage U_{loop}. The increasing loop voltage accelerates electrons produced by the pre-ionization source and avalanche ionization of the working gas occurs. After some delay, τ_{BD} ~ 1—2 ms, the plasma density becomes sufficiently high, and the plasma breakdown happens and plasma current starts to increase. At that time, the loop voltage reaches a maximum value U_{BD} and then drops dramatically. Later on, the discharge evolves spontaneously, since no control system for plasma current and plasma column displacement is available on GOLEM during this experiment. The discharge terminates by a sharp drop of the plasma current. The time interval between the breakdown time and termination of the plasma current is taken as the discharge duration T_{dis}. The plasma current increases during the discharge and in some moment reaches its maximum, $I_{pl_{max}}$. In this study, we take this time as a reference to compare various experimental plasma parameters. Fig. 4 highlights the differences between plasma parameters (black line — loop voltage, red line — plasma current,

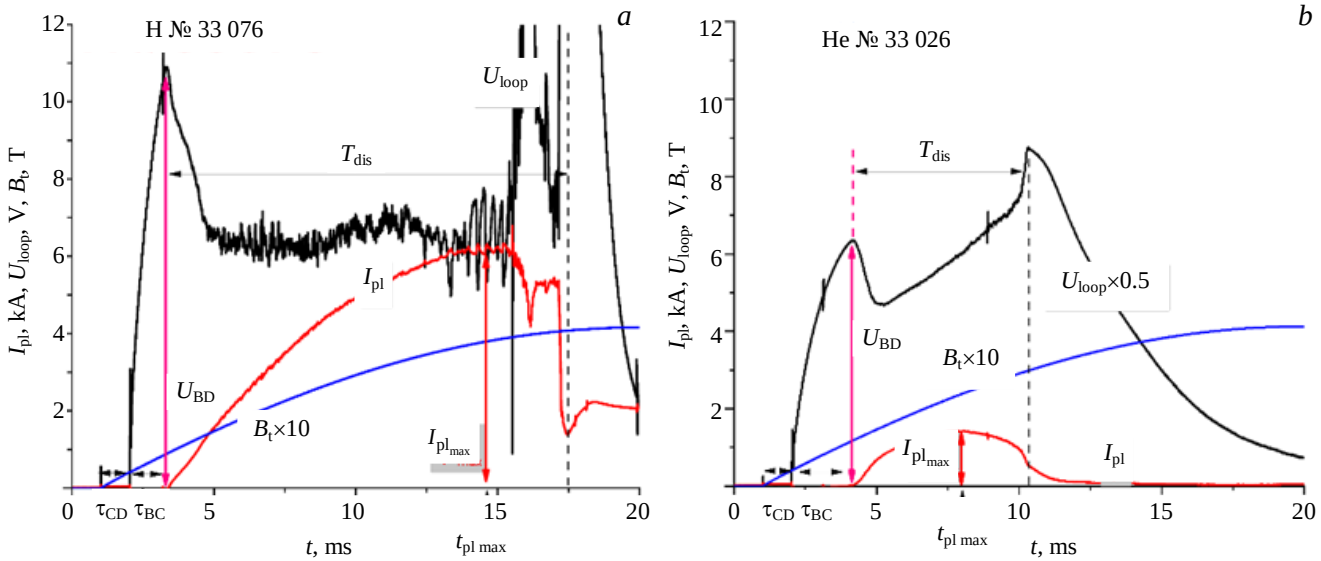

Fig. 4. Temporal evolution of the hydrogen (*a*), helium (*b*) discharge parameters

blue line — toroidal magnetic field) for the same scenario in hydrogen and helium plasmas. Further, unless otherwise stated, hydrogen data will be associated with red color, and helium data with blue.

EXPERIMENTAL RESULTS

Breakdown studies. Some features of breakdown progress on the GOLEM tokamak in hydrogen were studied in [20]. Here we focus on the comparison of breakdown in hydrogen and helium working gas. The time-traces of the main plasma parameters (plasma current, loop voltage and signal of visible emission diagnostics) are shown in fig. 5.

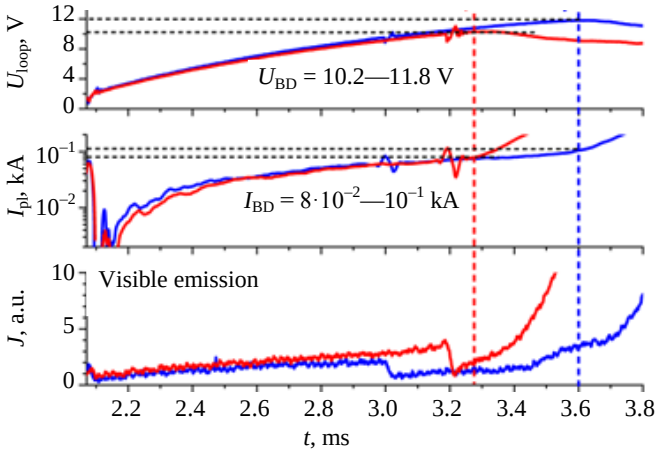

Fig. 5. Plasma start-up for two similar discharges executed at U_{CD} = 500 V. The working gas pressure is p_H = 27 mPa, p_{He} = 31.5 mPa. (Fast jumps on all signals at t = 3.0 and 3.2 ms appears due to machine power supplies triggers on the GOLEM data acquisition system): —— — H № 33 074; —— — He № 33 020; - - -, - - - — breakdown

The loop voltage applied at t = 2.1 ms causes the electrons acceleration along magnetic field lines by the toroidal electric field $E_t = \frac{U_{loop}}{2\pi R}$ to a drift velocity $v_D \propto E_t/p$, where p is the gas pressure. Once their energy exceeds the ionization energy of the working gas molecules/atoms, the electron density n_e and the plasma current $I_{pl} \sim n_e v_D$ increases. The initial fast increase of I_{pl} is slowed down because of charged particle losses, due to stray magnetic fields (in the range of 0.2 mT) and subsequent polarization of plasma column followed by fast convective losses [7, 28]. When $I_{pl} \geq 80$—100 A, its poloidal magnetic field becomes comparable with stray magnetic fields, the particle losses are dramatically reduced, and plasma current starts to increase much faster. The plasma resistivity $R_{pl} \sim \frac{U_{loop}}{I_{pl}} \approx 100$ mΩ, becomes a non-negligible fraction of the resistivity of the GOLEM vessel, $R_v \approx 10$ mΩ. Consequently, the loop voltage starts to decrease.

Fig. 5 shows the similarity in hydrogen and helium plasmas. The only visible difference is a longer avalanche phase in helium and consequent a higher breakdown voltage. This might be caused by differences electron drift velocities, gas pressures and first Townsend coefficient in hydrogen and helium. Scaling of the breakdown voltage with the working gas pressure is shown in fig. 6.

The full lines are polynomial fits of all data to guide the eye. Fig. 6 shows that the optimum range of pressures to get the lowest breakdown voltage is between 20—50 mPa for both hydrogen and helium, where the breakdown voltage is between 10—13 V. Note also that the data and in particular fit for hydrogen is consistent with the Paschen curve $U_{BD} = \frac{A 2\pi R p}{\ln 2\pi R p + B}$, where R is the major radius, A and B are first and second Townsend coefficients.

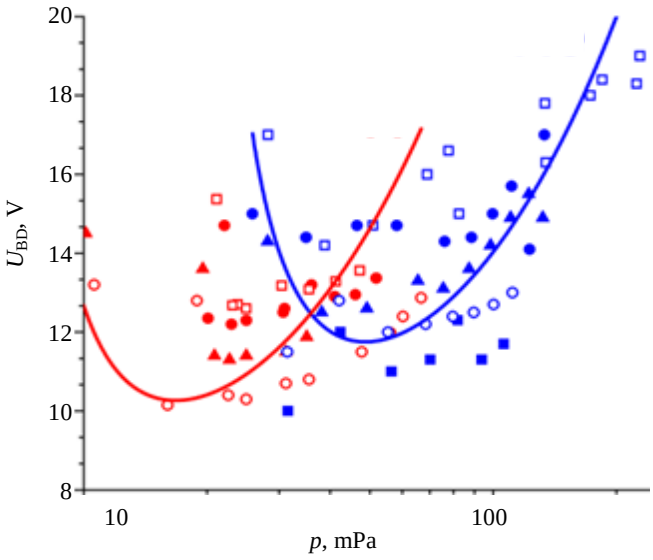

Fig. 6. Dependency of the breakdown voltage on the gas pressure for various U_{CD}: ■ — 400, ○ — 500, ▲ — 600, ● — 700, □ — 750 V; —— — H, —— — He

Discharge duration. Duration of discharge is an important parameter on GOLEM. It has to be maximized

(or optimized) to get sufficiently long time for any physical experiments. Fig. 7 compares the discharge duration in hydrogen and helium plasmas.

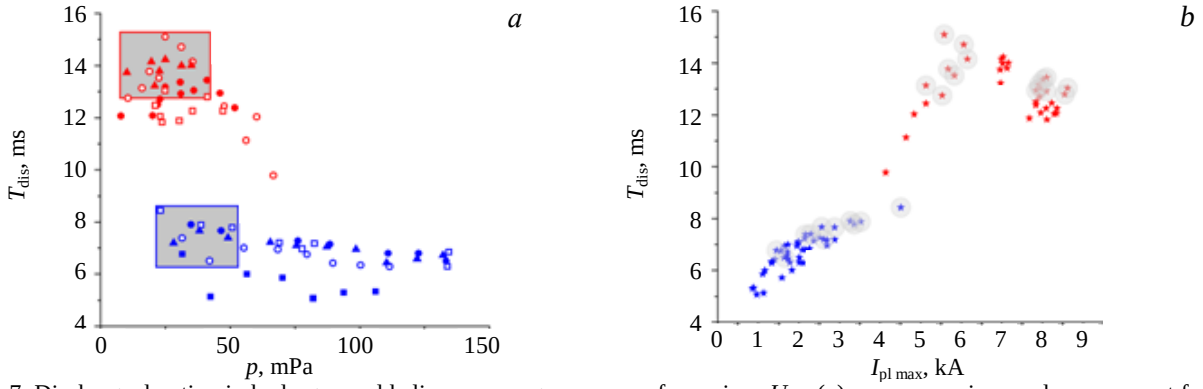

Fig. 7. Discharge duration in hydrogen and helium versus gas pressure for various U_{CD} (*a*); versus maximum plasma current for all U_{CD} (*b*): ■ — H, ■ — He

Experiment shows that discharge duration in hydrogen plasmas is noticeably longer than in helium plasmas by a factor of 2, and it slightly reduces when the gas pressure increases.

The shadowed rectangular areas (see fig. 7, *a*) and gray circles (see fig. 7, *b*) show roughly the optimum parameters to achieve longer discharge:

— hydrogen — p_H = 10—35 mPa, U_{CD} = 500—600 V;

— helium — p_{He} = 20—50 mPa, U_{CD} = 600—750 V.

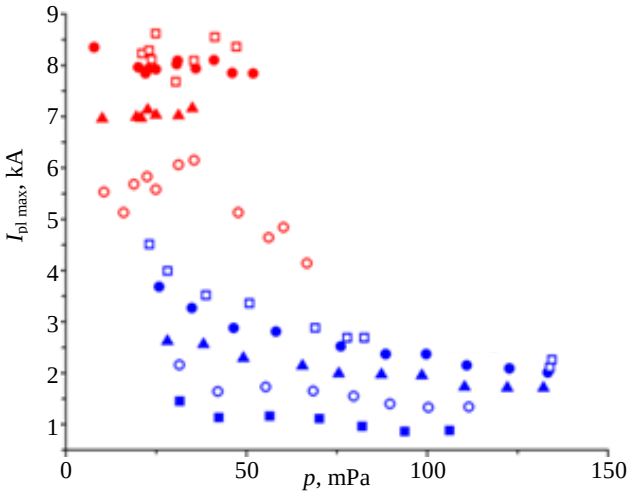

Fig. 8. Dependency of the maximum plasma current on the gas pressure for various U_{CD}: ■ — 400, ○ — 500, ▲ — 600, ● — 700, □ — 750 V; ■ — H, ■ — He

The rectangular areas in fig. 7 are just illustrative to show pressure ranges for getting a long discharge on GOLEM. In fact, duration depends strongly on the preparation of the inner wall of the vessel.

Maximum plasma current. Fig. 8 shows the maximum plasma current dependence on the working gas pressure for a various voltages applied to primary winding of the GOLEM transformer U_{CD}.

We clearly observe a decrease of the maximum current $I_{pl_{max}}$ with the pressure in both H- and He-plasmas. This might be caused by the fact that the plasma of GOLEM is not fully ionized and the degree of ionization decreases with the gas pressure. In addition, a systematic increase of the maximum current with U_{CD} is observed for both helium and hydrogen plasmas.

The ohmic heating power. The ohmic heating power is calculated as: $P_{OH} = U_{loop} I_{pl_{max}}$, where U_{loop} is the mean loop voltage averaged over T_{dis}. Ohmic heating power scan is plotted in fig. 9.

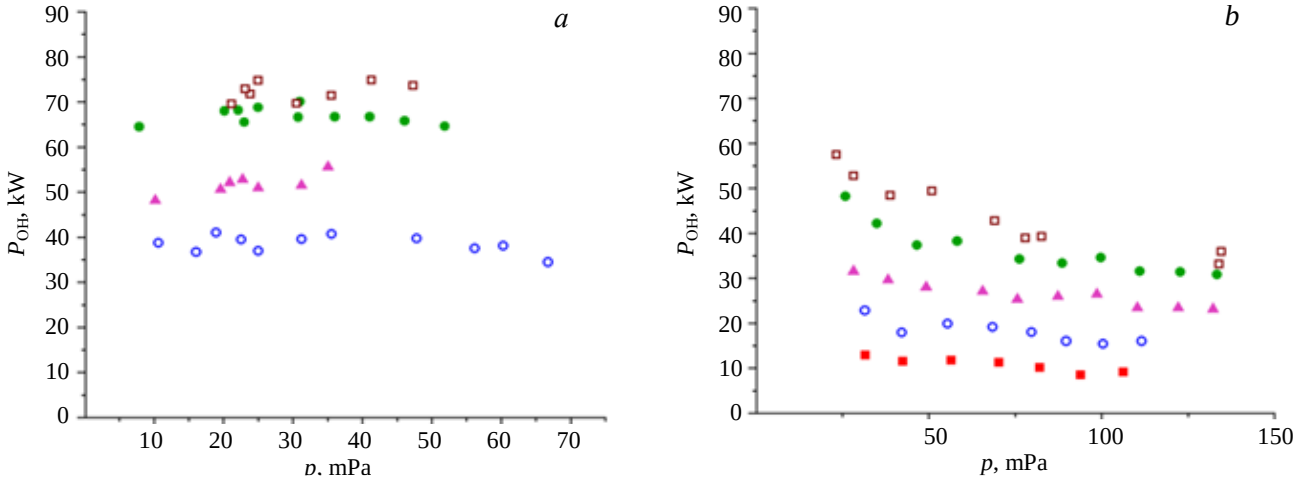

Fig. 9. Ohmic heating power versus working gas pressure for hydrogen: ■ — 400, ○ — 500, ▲ — 600, ● — 700, □ — 750 V (*a*); helium discharges (*b*)

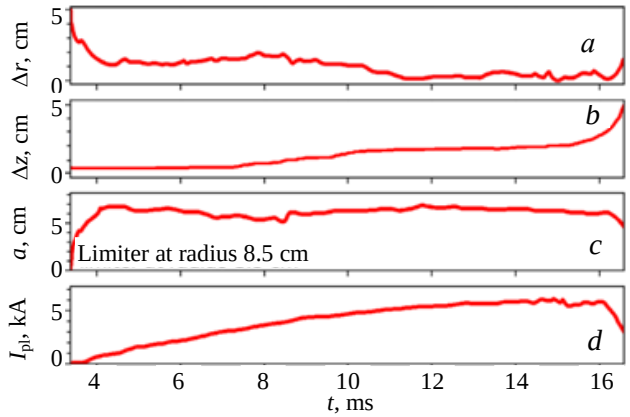

Fig. 10. Temporal evolutions of the radial (*a*), and vertical (*b*) displacement of the plasma column, resulting plasma minor radius (*c*) and plasma current (*d*), H № 33 073, U_{CD} = 500 V, *p* = 24 mPa

Almost no dependence of P_{OH} on the pressure is observed in both cases. Ohmic heating power in hydrogen plasmas is higher than in helium up to a factor of 2, due to higher maximum plasma current.

Displacement of the plasma column and edge safety factor. Plasma position in the GOLEM tokamak is not controlled by any external vertical/horizontal magnetic fields and evolves spontaneously during a discharge. Therefore, the plasma column may not be ideally centered during the discharge. The displacement of the plasma column was routinely derived for means of Mirnov Coils. A typical temporal evolution of the radial and vertical displacement is shown in fig. 10.

The radial displacement Δ*r* tends to reduce from a few cm up to zero, so the plasma column moves inward during the discharge. This is in contrast with the usual picture of toroidal discharges in other tokamaks, where Δ*r* > 0 due to the Ampere force and the increase of plasma pressure (ballooning effect). We suggest that the possible reason of such behavior of GOLEM plasmas can be a dominant attractive force of the iron core transformer.

In addition, we observe a positive displacement of plasma in the vertical direction Δ*z* during a discharge. The possible reason can be stray radial magnetic field, for example produced by misalignment of the toroidal field coils, which grows up during the discharge.

To compare displacements Δ*r*, Δ*z* over all considered discharges we take the maximum current time as a reference. Δ*r* and Δ*z* were averaged over 20 μs around the maximum plasma current. Their dependencies on the working gas pressure are plotted in fig. 11. It could be seen, that helium plasma never fills the entire chamber, independently from the gas pressure.

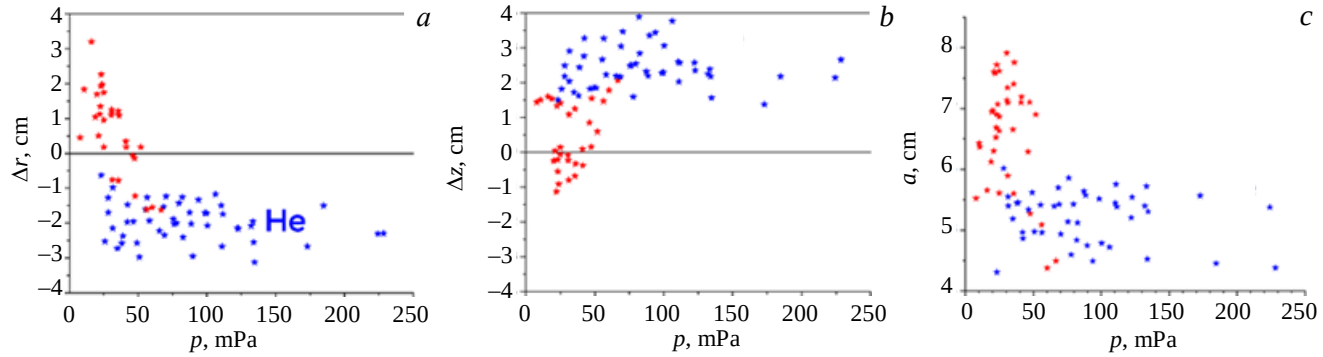

Fig. 11. Pressure scans for plasma displacement, horizontal (*a*), vertical (*b*), plasmas minor radius (*c*). Combined data for various U_{CD}: ■ — H, ■ — He

It is clearly seen that the displacements are independent from pressure for helium plasmas, while for hydrogen plasma the trend is not pronounced. Helium plasma column is always located inwards by ~2 cm and upwards by ~2 cm. The scan of displacements over the maximum plasma current is shown in fig. 12.

Plasma current position becomes more downward and inward shifted for helium shots, which is not the case for hydrogen shots. Hydrogen plasmas have a tendency for more central location. The general trend is a more centered column with the increase of the plasma current, and the central position is reached in hydrogen plasma.

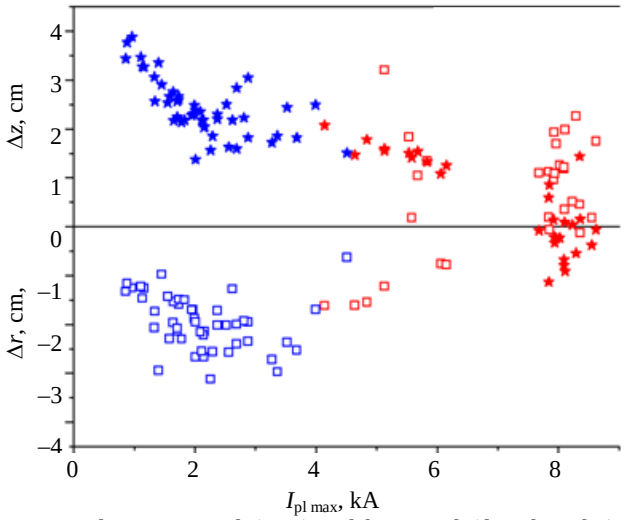

Fig. 12. Plasmas vertical (stars) and horizontal (dotted circles) displacement versus maximum plasma current Combined data for various U_{CD}: □ — horizontal (*r*), ★ — vertical (*z*), ■ — H, ■ — He

Central electron temperature. The central electron temperature is estimated from Spitzer conductivity as:

$$T_e(0) = 0.0163\left(\frac{Z_{\text{eff}} I_{\text{pl}}}{U_{\text{loop}} a^2}\right)^{2/3} \quad \text{[eV, m, kA, V]}, \tag{6}$$

where $T_e(r)$ is the electron temperature at radius r, a is the minor plasma radius, Z_{eff} is the effective plasma charge, and the center of plasma column is at $r = 0$. We estimate $Z_{\text{eff}} = 4$ for helium, and $Z_{\text{eff}} = 2.5$ for hydrogen plasmas. For $T_e(0)$ estimations the plasma minor radius was calculated using the data of the plasma vertical and horizontal shifts (see eq. (2), (3)). Fig. 13 shows the estimates for $T_e(0)$ taken for maximum plasma current.

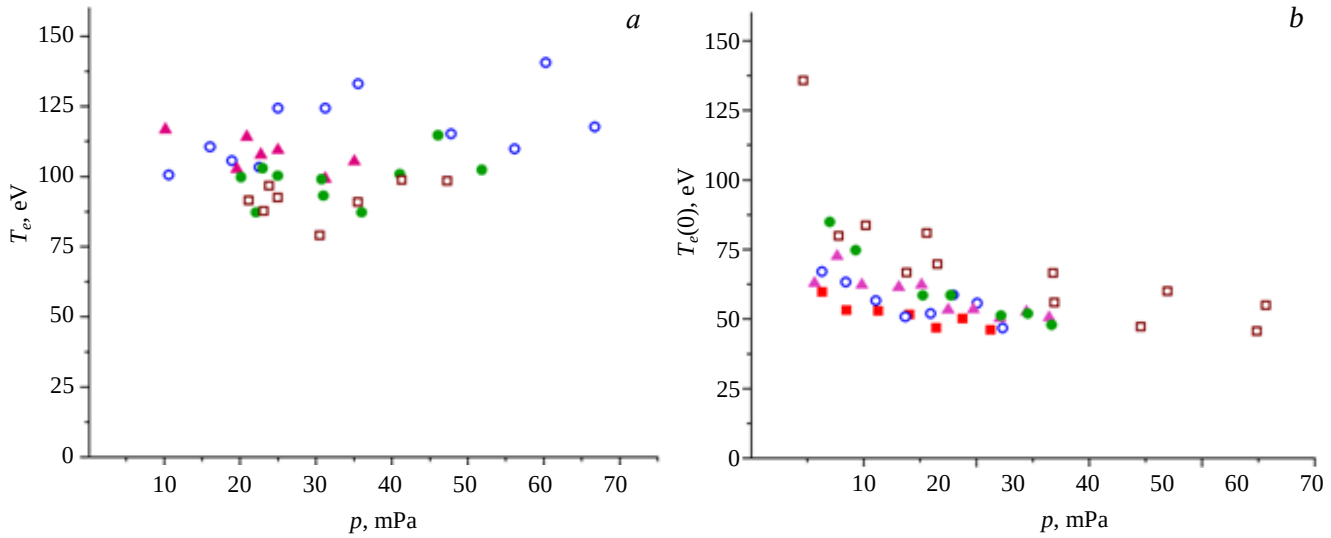

Fig. 13. Dependence of the central electron temperature on the pressure for different current drive voltages in hydrogen (*a*) and helium (*b*) discharges hydrogen: ■ — 400, ○ — 500, ▲ — 600, ● — 700, □ — 750 V

Fig. 13 shows that in hydrogen plasmas $T_e(0)$ is a factor of 1.5 larger due to larger $I_{\text{pl}_{\text{max}}}$. Helium plasma shows the systematic decay of the $I_{\text{pl}_{\text{max}}}$ with initial gas pressure, which is not the case for hydrogen plasma, where the dependence is not clear.

Electron temperature at the plasma edge. Edge electron temperature $T_e(a)$ was measured by electric probes. Fig. 14 shows time-traces of $T_e(a)$.

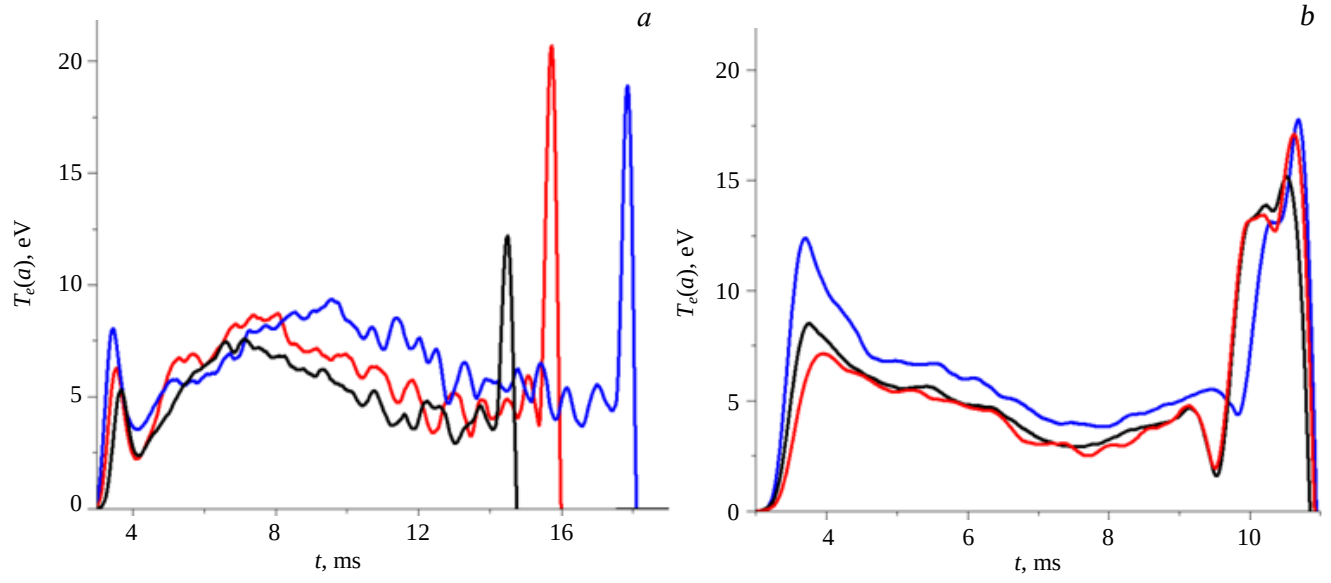

Fig. 14. Time evolution of the edge electron temperature for hydrogen: — № 33 067, p = 65, — № 33 065, p = 56, — № 33 075, p = 31 mPa, (*a*); helium plasmas: — № 33 023, p = 68, — № 33 022, p = 55, —№ 33 020, p = 31 mPa (*b*), as measured by Langmuir probe for shots with U_{CD} = 500 V

The absolute values of the edge temperatures happen to be close for hydrogen and helium plasmas, having the range of several eV and pronounced dynamics during the discharge. Fig. 15 shows that the edge temperature depends on the current drive voltage.

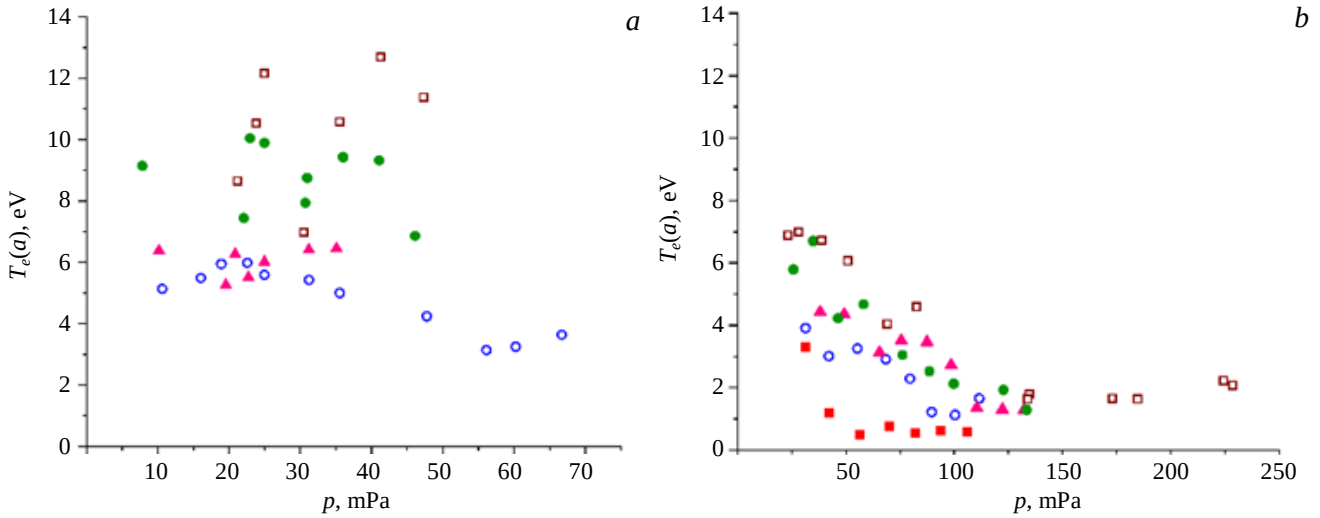

Fig. 15. Edge electron temperature dependencies on initial gas pressure and current drive voltage at the moment of maximum plasma current in (*a*) hydrogen (*b*) helium discharge: ■ — 400, ○ — 500, ▲ — 600, ● — 700, □ — 750 V

As far as helium mass is four times and charge is two times larger than hydrogen, radiative losses from helium plasma are larger. This explains the lower electron temperature in He plasmas compared to H in both core (see fig. 13) and edge (see fig. 15). The current drive voltage directly affects the plasma current. As GOLEM has only ohmic heating, the current (or U_{CD}) increase leads to an increase of the edge electron temperature, as shown in the fig. 15 and core electron temperature, as shown in the fig. 13.

Fig. 16 presents the edge electron temperature as a function of plasma current. The major trend is clear: the higher the current, the higher the edge electron temperature. This tendency is in line with the expectation for ohmically heated plasmas with a plasma current as the only source of thermal energy.

Interestingly, for the interval of current overlapping for hydrogen and helium plasmas (4 kA < $I_{pl_{max}}$ < 5 kA), edge electron temperature for helium plasmas is substantially (for a factor of 2) higher, than for hydrogen plasmas.

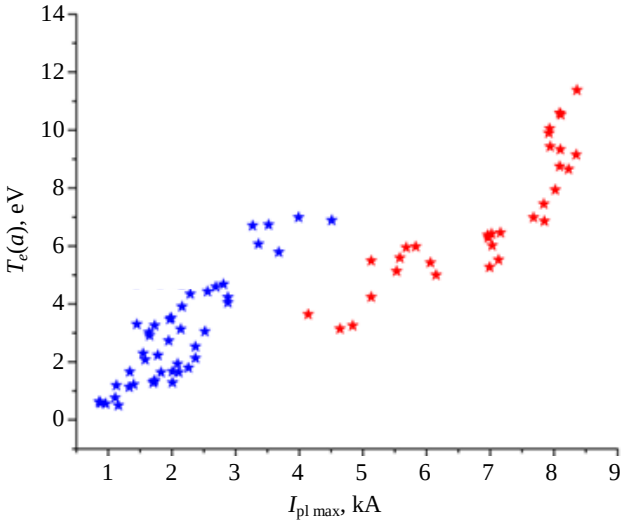

Fig. 16. Edge electron temperature versus maximum plasma current for all set of discharges with various current drive voltage U_{CD}. The edge electron temperatures were taken at the moment of maximum plasma current. Combined data for various U_{CD}: ■ — H, ■ — He

Electron energy confinement time analysis. The global energy confinement time τ_e is defined as

$$\tau_e = \frac{W_e}{P_{OH}} \text{ [s, J, W]}, \qquad (7)$$

where $W_e = \int_{V_p} n_e T_e dV$ is the total energy in the plasma column of the volume $V_p = 2\pi^2 R a^2$. Determination of W_e requires knowledge of radial profiles of $T_e(r)$ and $n_e(r)$, which are not measured at GOLEM. To describe scaling of τ_e on measurable quantities, in particular on the pressure of the gas $p = k_B n_e T_{gas}$ we are limiting n_e as for fully ionized plasma provided by injected gas with temperature T_{gas}. For hydrogen plasma the value should be multiplied by a factor of 2 because of dissociation $H_2 \rightarrow 2H$. We approximate $W_e = \frac{3}{8} T_e(0) n_e V_p$ (where 3/2 comes from degrees of freedom and 1/4 comes from

averaging n_eT_e) [29]. Therefore, the electron energy confinement $\tau_e^{\exp}$ scales with the pressure as (a, $T_e(0)$ and U_{loop} are taken at the moment of $I_{\text{pl}_{\max}}$):

$$\tau_e^{\exp} = \frac{6\pi^2 R}{8k_B T_{\text{gas}}} \frac{a^2 T_e(0) p}{U_{\text{loop}} I_{\text{pl}_{\max}}} \text{ [s, m, m}^2\text{, K, Pa, K, V, A]}, \quad (8)$$

τ_e dependence on the gas pressure for helium and hydrogen plasmas is shown in fig. 17.

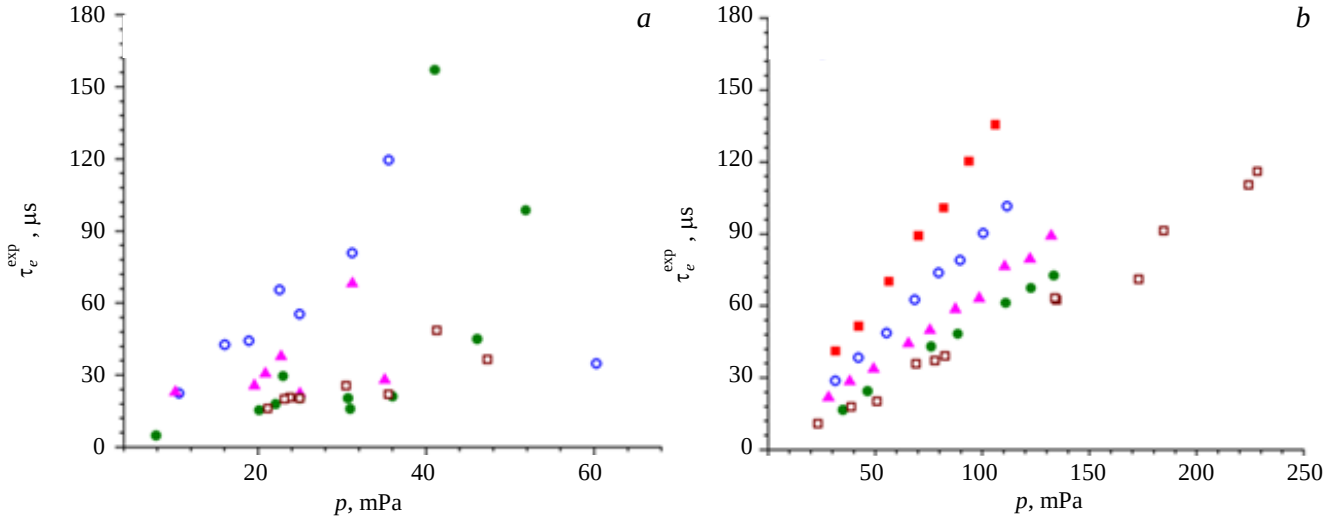

Fig. 17. Global electron energy confinement time versus initial gas pressure for hydrogen (*a*) and helium (*b*) discharges, U_{CD}: ■ — 400, ○ — 500, ▲ — 600, ● — 700, □ — 750 V

We observe a linear increase of τ_e with the pressure (density) in both cases. Decreasing of τ_e with increase of U_{CD} is clearly seen in helium shots, which implies a dependency on the plasma current.

It is interesting to compare our data with existing scaling of the global energy confinement time [30], where results from a number of experimental devices were compiled, and an overall scaling law for ohmically heated tokamaks was deduced:

$$\tau_e \sim n_e a^2 \sqrt{q} \text{ [s, m}^{-3}\text{, m}^2\text{]}.$$

Alternatively, Neo-Alcator scaling was proposed [31]:

$$\tau_e = 1.92 \cdot 10^{-21} R^{2.04} a^{1.04} n_e \text{ [s, m, m, m}^{-3}\text{]}. \quad (9)$$

Scaling law of electron energy confinement time on GOLEM was found as [32]:

$$\tau_e^{\text{GOLEM}} = 3 \cdot 10^{-22} I_{\text{pl}}^{0.95} B_{\text{t}}^{0.31} P_{\text{OH}}^{-1.33} n_e^{1.04} \text{ [s, A, T, W, m}^{-3}\text{]}. \quad (10)$$

Fig. 18 shows that obtained regimes have about factor of 1.4 better confinement than prediction of the conventional GOLEM scaling for helium, while for hydrogen this factor is slightly lower, about 1.3. On the other

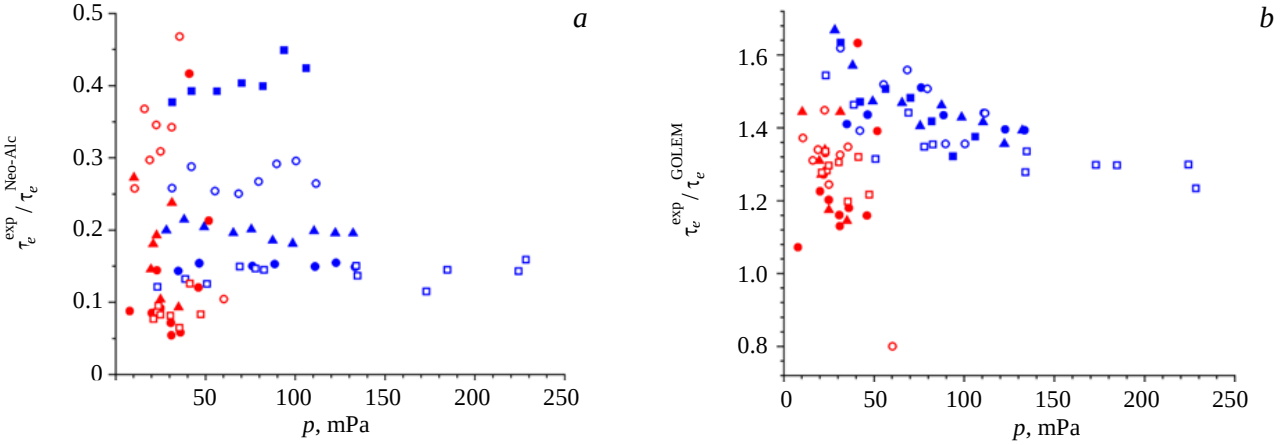

Fig. 18: Dependence of experimental and Neo-Alcator τ_e-scaling attitude (*a*) and experimental and GOLEM τ_e-scaling attitude dependence (*b*) on gas pressure, U_{CD}: ■ — 400, ○ — 500, ▲ — 600, ● — 700, □ — 750 V

hand, for both hydrogen and helium confinement on GOLEM is lower than prediction from Neo-Alcator scaling, based on the larger scale tokamaks.

Maximum available magnetic flux through the iron core transformer of GOLEM. The iron core transformer of GOLEM is designed to transport the maximum magnetic flux around Φ_{max} = 120 mWb [27]. The magnetic flux Φ through the central column of the GOLEM transformer can be calculated as the integral of the loop voltage

$$\Phi(t) = \int_0^t U_{loop}(\tau)d\tau \ \text{[Wb, V, s]}.$$

An example of temporal evolution of the loop voltage and resulting magnetic flux $\Phi(t)$ is plotted in fig. 19. An excellent agreement is seen in the determination of the end of the discharge by the plasma current and by the magnetic flux.

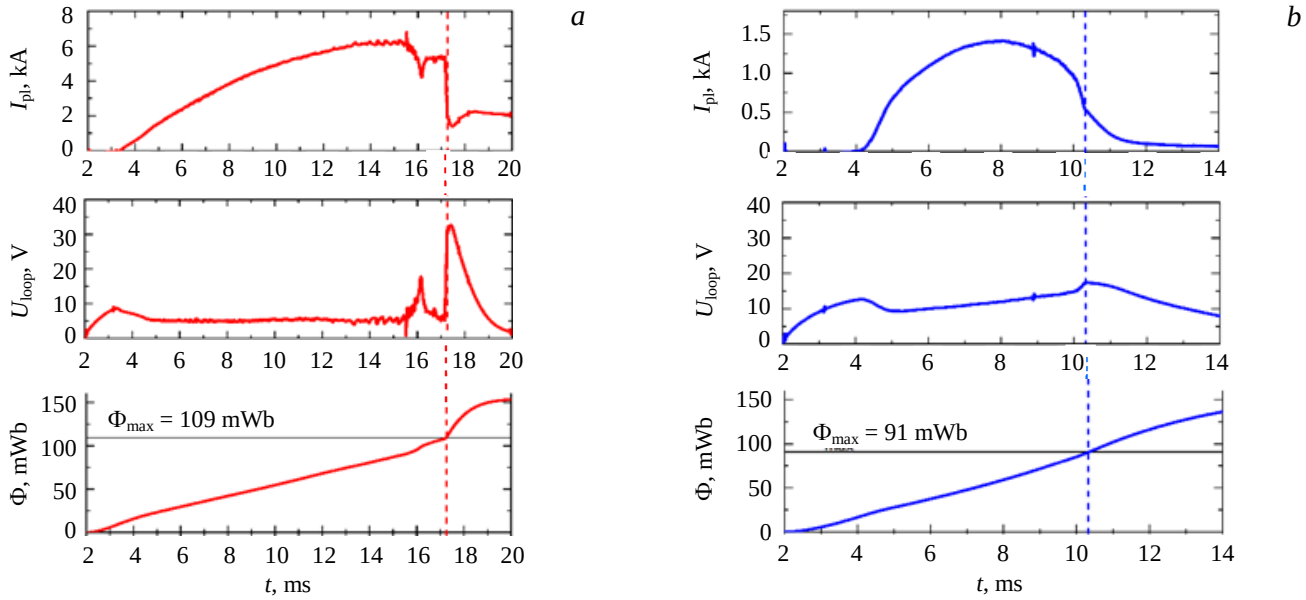

Fig. 19. Evolution of the plasma current, total magnetic flux and loop voltage for H- (№ 33 076) (*a*) and He-discharges (№ 33 026) (*b*) at U_{CD} = 500 V

It is evident that the duration is decreasing with the loop voltage during the plasma phase i.e., the lower loop voltage at the breakdown time is followed by a longer discharge. The loop voltage is proportional to the effective plasma charge Z_{eff}, which is higher for helium plasmas. This is the reason why the discharge duration T_{dis} in hydrogen plasmas is always longer than in helium ones. With a long vessel heating and glow discharge cleaning the discharge duration is always longer [21].

Note also that a noticeable magnetic flux (~20—25%) is already consumed before the breakdown, which shows an importance of optimization of the breakdown conditions for plasma performance.

Fig. 20 shows the magnetic flux limit of the GOLEM transformer, that is reached only at the highest U_{CD}, in particular in helium plasmas. On the other hand, the discharges at $U_{CD} \leq 500$—600 V are not terminated by a maximum magnetic flux of the transformer, and therefore we have to look for another mechanism, limiting the discharge duration.

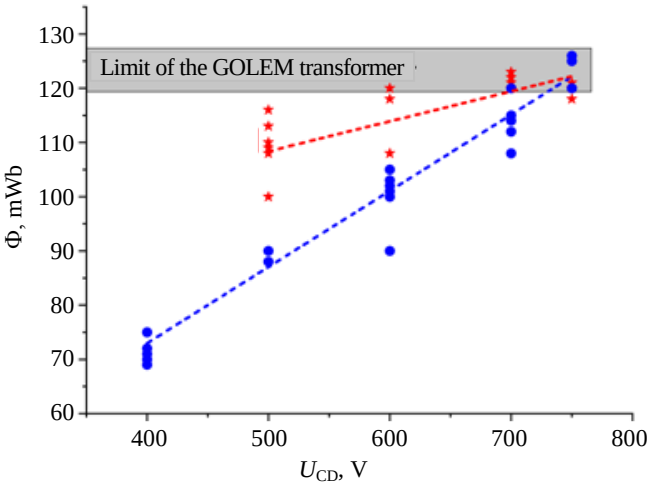

Fig. 20. Maximum magnetic flux versus the charging voltage in hydrogen (■) and helium (■) plasmas

Termination of the discharge by shrinking of plasma column and the decrease of the edge safety

factor. The edge safety factor q(a) at the maximum plasma current is:

$$q(a) = \frac{a B_{\text{t max}}}{R_0 B_{p\ \text{max}}} \sim \frac{a^2 B_{\text{t max}}}{R_0 I_{\text{pl max}}}, \qquad (11)$$

where $B_{\text{t max}}$ is the toroidal magnetic field at the maximum of the plasma current, plasma minor radius is calculated using the data on the horizontal and vertical displacement. Comparison of the discharge termination process at approximately the same gas pressure and the same current drive voltage could be provided.

A possible reason for the discharge termination can be the formation of MHD-modes, which can lead to macroscopic instabilities preceding the breakdown. Because of these instabilities, which are noticed in the form of irregular oscillations and then drops in the plasma current, the duration of hydrogen discharges exhibits a kind of random nature due to the inaccuracy of determining the end of the discharge. On the contrary, no significant magnetic instabilities were observed in helium discharges.

Fig. 21 shows the development of a single breakdown of the plasma current, which led to the end of the discharge. This development of events is typical for high gas pressure.

Here it is possible to determine the value of the safety factor at the plasma boundary $q(a)$ at the moment of this instability. For hydrogen discharges, the minimum $q(a)$ is limited to 2, which indicates that sawtooth oscillations are observed, fig. 22.

At the maximum of reached plasma current in helium (U_{CD} = 750 V), as well as at the minimum of plasma current in hydrogen (U_{CD} = 500 V), some disturbances are observed, which can be identified with weak MHD-instability (fig. 23). Due to the in-

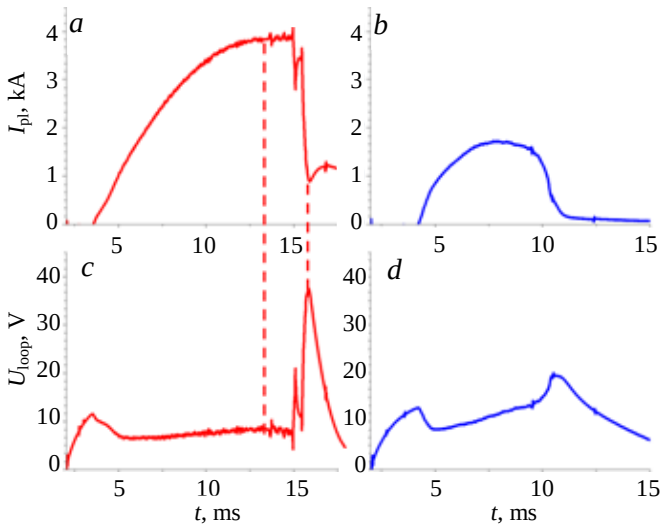

Fig. 21. Presence of macroscopic MHD-instability on loop voltage (*a*, *b*) and plasma current (*c*, *d*) in H- (# 33 066), U_{CD} = 500 V, p = 48 mPa (*a*, *c*) and absence in He-discharges (# 33 021), U_{CD} = 500 V, p = 42 mPa (*c*, *d*). Such fast oscillations indicate MHD-instabilities

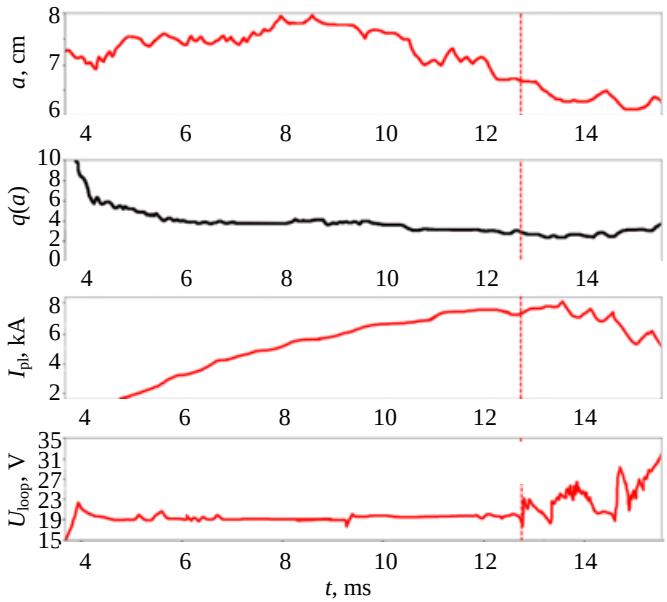

Fig. 22. Excitation of MHD-instability at the final stage of in hydrogen discharges, when edge safety factor approaches 2, № 33 093

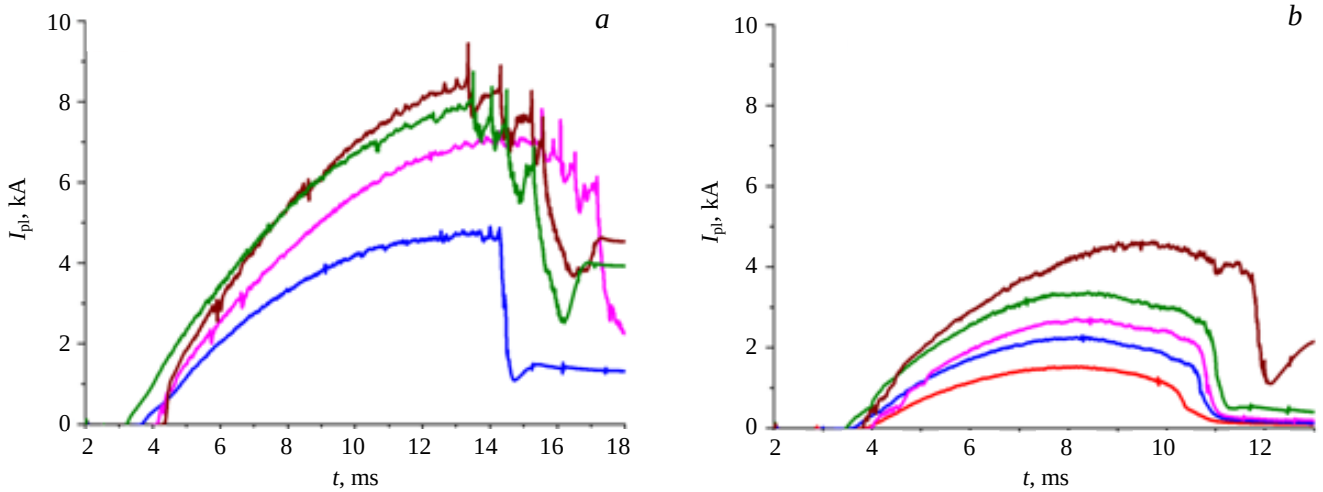

Fig. 23. Evolution of the plasma current in hydrogen (*a*) and helium (*b*) plasmas for several charging voltages U_{CD}: — — 400, — — 500, — — 600, — — 700, — — 750 V

crease in the plasma current and the compression of the plasma column due to a displacement of its axis, the edge safety factor $q(a)$ falls below 2, which leads to the development of MHD-instability. For hydrogen, this effect is more notable than for helium. It seems that the helium discharge with the largest current drive is similar to the hydrogen discharge with the lowest.

Analysis of magnetic fluctuations measured by Mirnov Coils. Fast Fourier transform (FFT) technique was used to analyze magnetic oscillations. For the Fourier transform $\mathrm{F}(f)$ of the signals (time series) the power spectrum or power spectral density (PSD) is defined as: $P_{11}(f) = \mathrm{F}_1(f)\mathrm{F}_1^*(f)$ where the asterisk denotes a complex conjugate. For two different signals with $\mathrm{F}_1(f), \mathrm{F}_2(f)$ the cross-spectrum is defined as: $P_{12}(f) = \mathrm{F}_1(f)\mathrm{F}_2^*(f)$. In general, $P_{12}(f)$ is a complex function, so it may be presented as follows:

$$P_{12}(f) = |P_{12}(f)| e^{i\Phi_{12}(f)}, \tag{12}$$

where $|P_{12}(f)|$ is absolute value of cross-spectrum and $\Phi_{12}(f,\ t) = \mathrm{arctg}\left\{\dfrac{\mathbf{Im}(P_{12})}{\mathbf{Re}(P_{12})}\right\}$ is cross-phase between two signals.

The coherence between two signals is the normalized cross-spectrum [33]:

$$C_{12}(f) = \frac{|P_{12}(f)|}{\sqrt{P_{11}(f)P_{22}(f)}}. \tag{13}$$

An example of power spectrograms for magnetic signals of Mirnov Coils is shown in fig. 24 together with plasma current and loop voltage during whole discharge. Time-averaged PSD for chosen time periods is shown near each spectrogram. A coherent fluctuation of magnetic field with the maximum amplitude at $f \sim 25$ kHz is excited from 8 ms up to the appearance of plasma current oscillations at the final stage of the discharge around 13 ms.

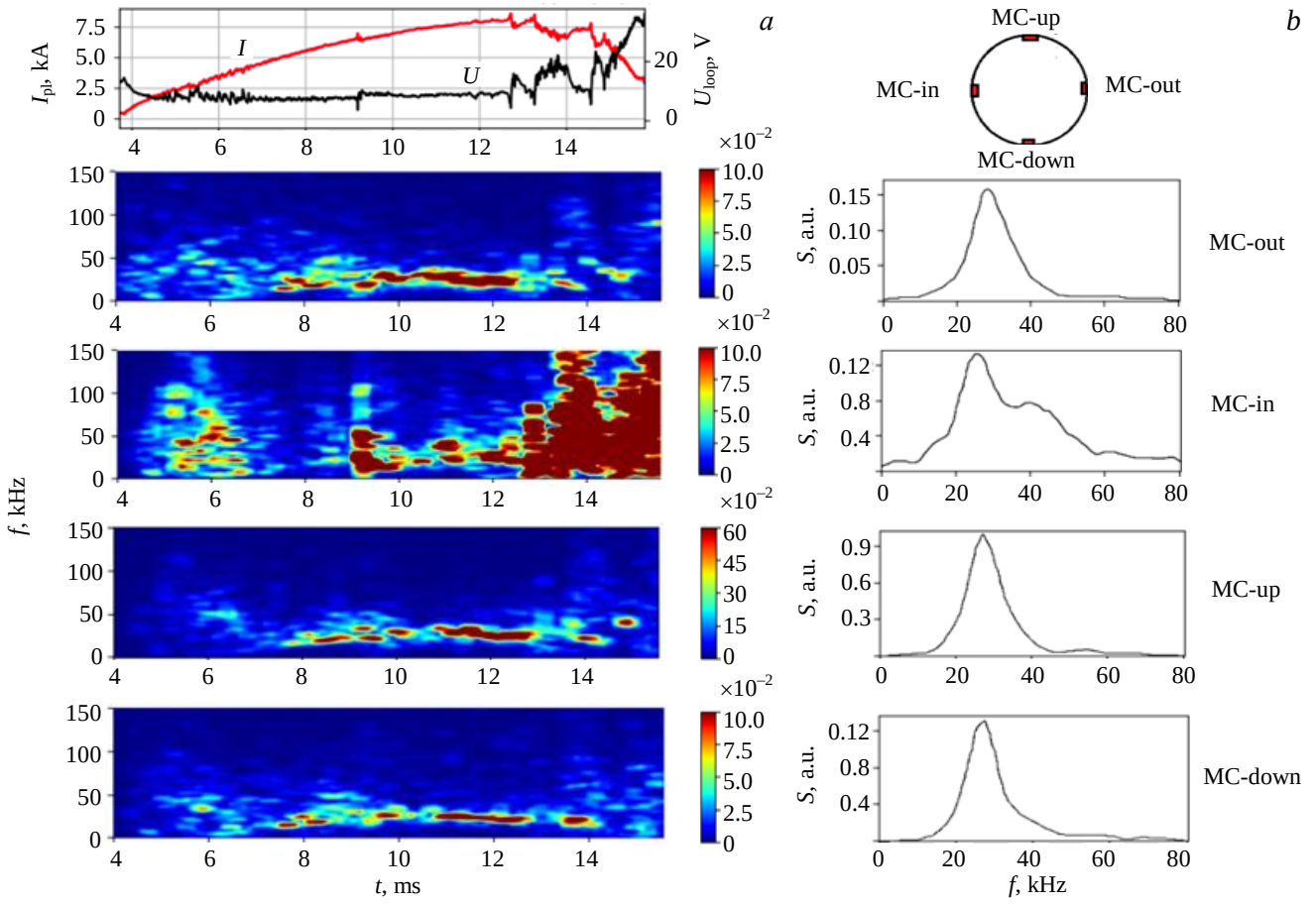

Fig. 24. Power spectrograms, H № 33 087 (*a*) and time-averaged (10 ms < *t* < 12.5 ms) power spectra (*b*) of the Mirnov Coil signals. Coherent magnetic fluctuation is excited in the range 20—40 kHz

However, the coil MC-in less clearly reproduces such coherent fluctuations, but shows some broadband turbulence at the final stage of the discharge. The results of cross-coherence between MC signals are shown in fig. 25.

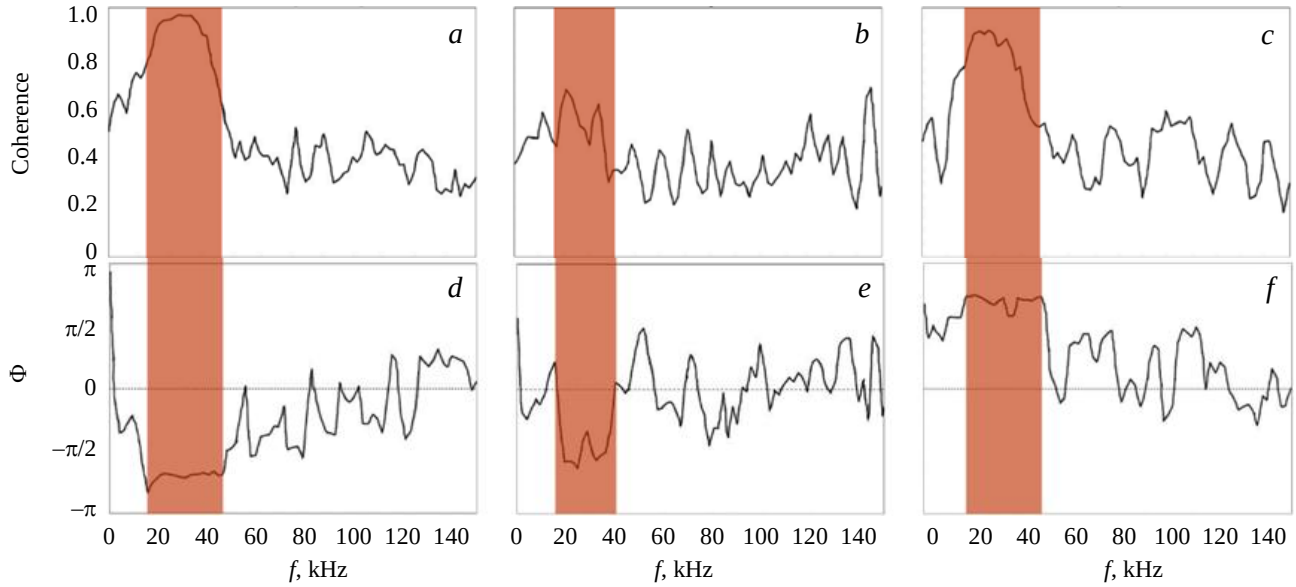

Fig. 25. Cross-coherence (*a*) and cross-phase (*b*) for shot № 33 087. Coherent magnetic fluctuation in the range 20—40 kHz has statistically valuable coherence and non-random cross-phase, time window: $10.0 < t < 12.5$, MC-out|MC-up — *a*, *d*; MC-out|MC-in — *b*, *e*; MC-out|MC-down — *c*, *f*

Top series of graphs shows high coherency at $f \sim 20$—40 kHz for coil pairs MC-out|MC-up and MC-out|MC-down. The coherence MC-out|MC-in is lower, so only three signals MC-out, MC-up and MC-down were used for poloidal mode number m reconstruction. Cross-phases for each pair of coils represents phase for the second coil in the pair for zero phase in the first coil. Fig. 25 shows the following phases for signals (tab. 2).

T a b l e 2. **Phases for signals**

Mirnov Coil	MC-out	MC-up	MC-in	MC-down
Phase	0	–3π/4	–π	3π/4
Poloidal angle	0	π/2	π	–π/2

That represents the poloidal mode number $m = 3$ for this instability.

In contrast to H-shots the He-shots show a sort of quasi-coherent fluctuations in the range 30—150 kHz, which present a hot topic for plasma research in the medium-size machines [34—36] as well as in small devices [37—39]. An example of spectrogram is shown in fig. 26. Figure shows the quiescent period in the phase of the

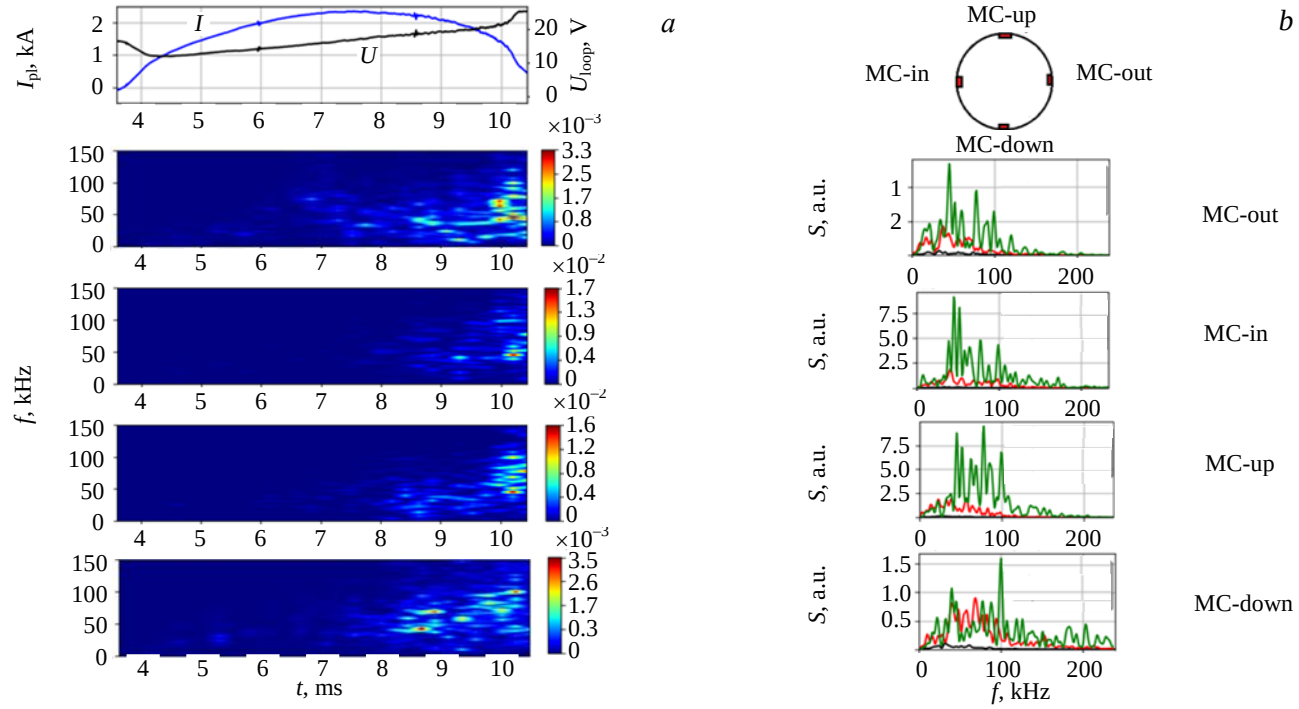

Fig. 26. Power spectrograms, H № 33 052 (*a*) and time-averaged power spectra, — — $3.6 < t < 8.0$; — — $8.0 < t < 10.0$; — — $10.0 < t < 10.4$; (*b*) of the Mirnov Coil signals. Quasi-coherent magnetic fluctuation is excited in the range 30—150 kHz

I_{pl} raise (3.6—8 ms), then an appearance of quasi-coherent fluctuations (red curves) in the phase of the I_{pl} decay, and further development of some broadband turbulence at the very end of the discharge (green curves), again, resembling the observations from the medium-size machine [40, 41].

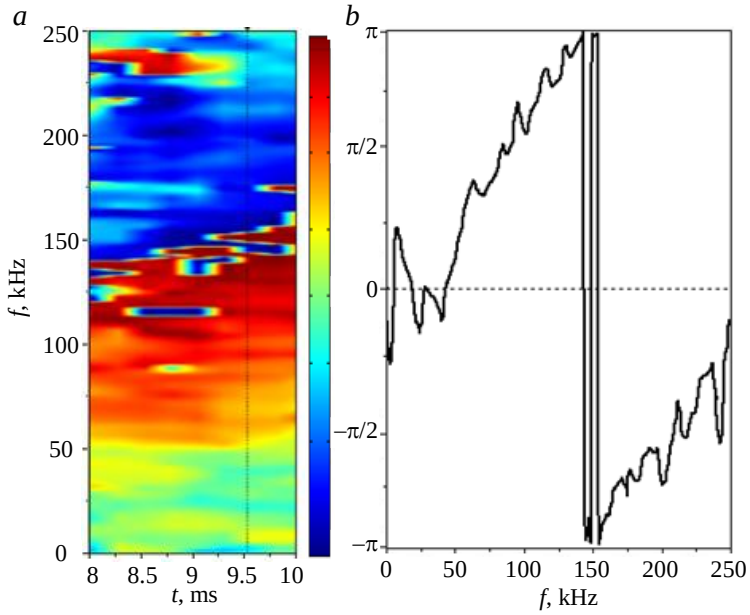

Fig. 27. Cross-phase spectrogram of MC-out|MC-down signals (*a*) and cross-phase spectrum for t = 9.51 ms (*b*), shot № 33 052

The analysis of the MC data gives the systematic structure of the cross-phase versus frequency in the stage of the I_{pl} decay (8 ms < t < 10 ms), as shown in the cross-phase spectrogram in fig. 27, *a*. The cross-phase dependence on frequency shown in fig. 27, *b* has a linear character. It resembles the direct propagation of broadband (0 < f < 250 kHz) magnetic perturbation from one probe to another one with a finite velocity. Remarkably, the cross-phase passes through π at 150 kHz and then continue the linear coupling. Note that the increase of the frequency, that passes π, from 120 kHz to 150 kHz indicates the increase in the turbulence rotation during considered time interval.

Fig. 28 shows two-dimensional frequency-cross-phase power spectra $S(\Phi, f)$ for broadband magnetic turbulence in typical hydrogen and helium discharges. It shows the coherent magnetic mode with the maximum amplitude at $f \sim 25$ kHz in hydrogen, see fig. 26, contrasting with a systematic linear-like structure along the line, starting from the origin (0, 0). The latter indicates the direct propagation of broadband (0 < f < 250 kHz) magnetic perturbation from one probe to another one. This poloidal propagation might be considered as a poloidal magnetic turbulence rotation with a finite velocity [42].

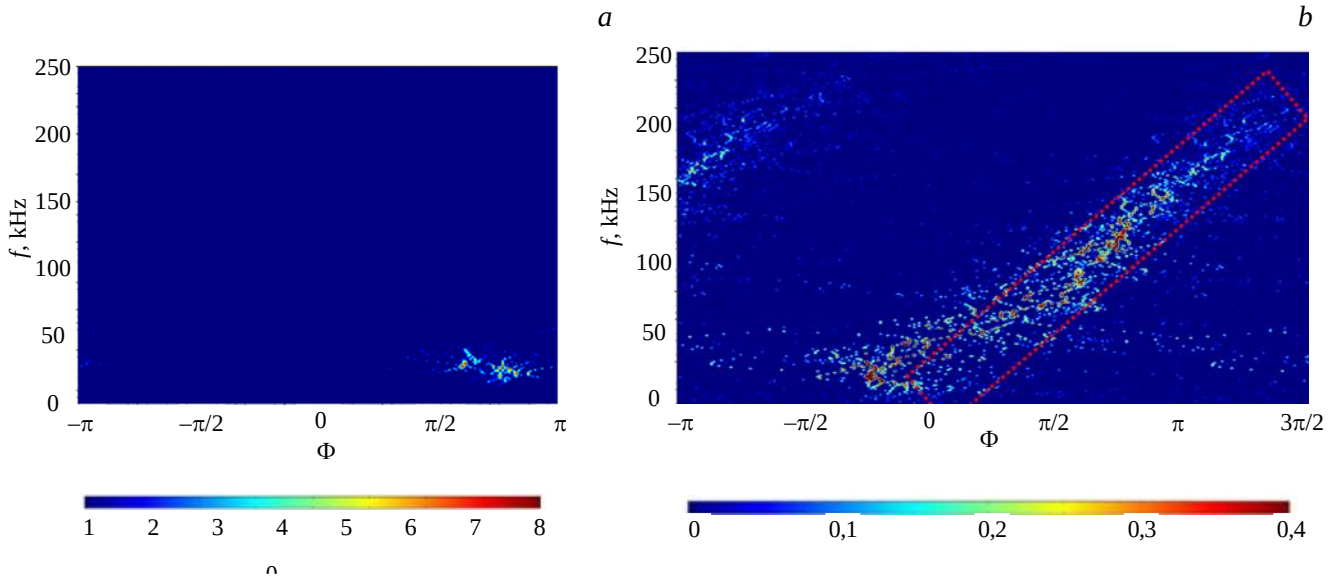

Fig. 28. Two-dimensional power spectra $S(\Phi, f)$ for broadband magnetic turbulence in typical hydrogen, № 33 087 (*a*) and helium, № 33 012 (*b*) discharge

Long-range correlations of the edge plasma fluctuations. Long-range correlations indicate any type of global mode of plasma oscillations including Geodesic Acoustic Modes [43]. Electric and magnetic probes in the GOLEM tokamak are located at a distance of a quarter of a torus and at different poloidal angles (see fig. 1).

Analysis of the coherence and cross-phases between the magnetic oscillations measured by Mirnov Coils and the floating potential oscillations measured by Langmuir probe is shown in fig. 29 and presents a mode with a frequency about 20—40 kHz, clearly visible on all four MCs, in most of hydrogen shots, as coherent magnetic fluctuation (see fig. 24, 25). These fluctuation is observed in the quiet stage of the discharge, when the plasma current has not yet reached its maximum and the quenching instabilities typical of a hydrogen discharge have not yet been excited. It should be mentioned that the long-range correlations sometimes occur in a more extended frequency range (20—60 kHz).

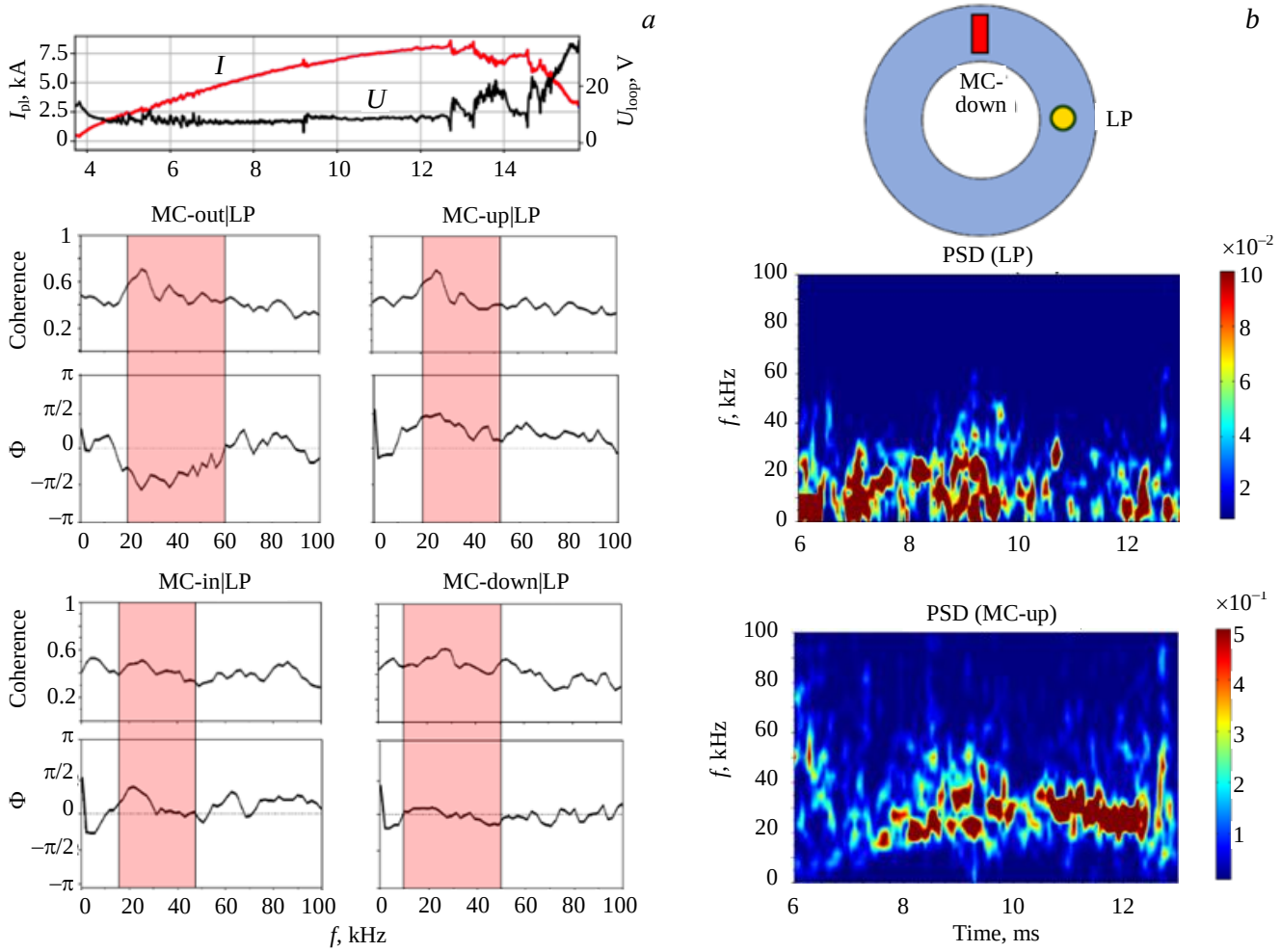

Fig. 29. Observation of the long-range correlation for coherent magnetic oscillations. Coherence and cross-phase between plasma potential by Langmuir probe and magnetic oscillations by Mirnov coils (*a*) averaged over 6 ms < *t* < 13 ms. The long-range coherence in the range 20—60 kHz exceeds the confidence level of 0.3. Power spectral density of Langmuir probe and one of MCs signals (*b*), H № 33 087

In contrast to a hydrogen discharge, a helium discharge develops without any noticeable long-range correlations.

SUMMARY

Experiments have shown that with the same preset discharge parameters (gas pressure, current drive voltage, magnetic field, etc.) plasma scenarios in hydrogen and in helium in GOLEM are radically different. In hydrogen plasma magnetic instabilities usually occur near the maximum plasma current, that lead to the disruption and plasma termination, while the helium plasma quietly extinguishes by itself due to the exhaust of the magnetic flux in the primary winding of tokamak transformer.

The main links between the plasma discharge parameters were confirmed: the discharge duration and electron temperature increase with plasma current, which in turn increases with gas pressure. In addition, electron energy confinement time exceeds τ_e scaling for GOLEM by a factor of 1.4. It is shown that there is a range of

pressure and voltage parameters of the current drive, where the main parameters of the discharge (edge and central electron temperatures, plasma current) are similar for both gases. However, on the whole, it can be concluded that the discharge energy in helium is lower than in hydrogen. However, it can be concluded that the absorption of the ohmic power is somewhat worse, because of this, in general, the parameters of helium discharges are lower than in hydrogen.

The presence of long-range toroidal/poloidal correlations between electric potential and magnetic perturbation was observed and the existence of broadband magnetic turbulence was demonstrated for the first time.

ACKNOWLEDGEMENTS

Authors would like to thank Ruslan Begishev, Mikhail Gorbun and Nikita Vadimov for participating in the experiments. GOLEM operation is supported by IAEA research contract F13019 «Network of Small and Medium Size Magnetic Confinement Fusion Devices for Fusion Research». MHD turbulence and long-range correlation studies were supported by Russian Science Foundation, project 19-12-00312.

REFERENCES

1. **Manas P., Angioni C., Kappatou A. et al.** The confinement of helium tokamak plasmas, impact of electron heating, turbulent transport and zonal flows. — Nucl. Fusion, 2019, vol. 59, p. 014002.
2. **Waltz R.E., Dewar R.L., Garbet X.** Theory and simulation of rotational shear stabilization of turbulence. — Phys. Plasmas, 1998, vol. 5, p. 1784.
3. **Van Oost G., Bulanin V.V., Donné A.J.H. et al.** Multi-machine studies of the role of turbulence and electric fields in the establishment of improved confinement in tokamak plasmas. — Plasma Phys. Control. Fusion, 2007, vol. 49, pp. A29—A44.
4. **Nakata M., Nunami M., Sugama H.** Multi-machine studies of the role of turbulence and electric fields in the establishment of improved confinement in tokamak plasmas. — Phys. Rev. Lett., 2017, vol. 118, p. 165002.
5. **Gryaznevich M., Van Oost G., Peleman P. et al.** Results of Joint Experiments and other IAEA activities on research using small tokamaks. — Nucl. Fusion, 2009, vol. 49, p. 104026.
6. **Van Oost G., Adámek J., Antoni V. et al.** Turbulent transport reduction by **E**×**B** velocity shear during edge plasma biasing: recent experimental results. — Plasma Phys. Control. Fusion, 2003, vol. 45, pp. 621—643.
7. **Gryaznevich M. et al.** Characteristics of the core and edge plasma turbulence in small Tokamaks. — Iranian Physical J., 2008, vol. 2—3, pp. 1—7.
8. **Gryaznevich M.P., Stöckel J., Van Oost G. et al.** Contribution of joint experiments on small tokamaks in the framework of IAEA Coordinated Research Projects to mainstream Fusion Research. — Plasma Sci. Technol., 2020, vol. 22, p. 055102.
9. **Van Oost G., Gryaznevich M., Del Bosco E. et al.** Joint experiments on the tokamaks CASTOR and T-10. — AIP Conf. Proc., 2008, vol. 996, p. 24.
10. **Van Oost G., Gunn J.P., Melnikov A. et al.** The role of radial electric fields in the tokamaks TEXTOR-94, CASTOR, and T-10. — Czechoslovak J. of Physics, 2001, vol. 51 (10), pp. 957—975.
11. **Gryaznevich M., Van Oost G, Stöckel J et al.** Contribution to fusion research from IAEA Coordinated Research Projects and Joint Experiments. — Nucl. Fusion, 2015, vol. 55, p. 104019.
12. **Fujisawa A. et al.** Experimental progress on zonal flow physics in toroidal plasmas. — Nucl. Fusion, 2007, vol. 47, p. S718.
13. **Melnikov A.V. et al.** Investigation of the plasma potential oscillations in the range of geodesic acoustic mode frequencies by heavy ion beam probing in tokamaks. — Czech. J. Phys., 2005, vol. 55, p. 349.
14. **Melnikov A.V. et al.** Correlation properties of geodesic acoustic modes in the T-10 tokamak. — J. Phys.: Conf. Ser., 2015, vol. 591, p. 012003.
15. **Melnikov A.V. et al.** Investigation of geodesic acoustic mode oscillations in the T-10 tokamak. — Plasma Phys. Control. Fusion, 2006, vol. 48, p. S87.
16. **Fujisawa A. et al.** Identification of zonal flows in a toroidal plasma. — Phys. Rev. Lett., 2004, vol. 93, p. 65002.
17. **Alonso J.A. et al.** Observation of oscillatory radial electric field relaxation in a helical plasma. — Phys. Rev. Lett., 2017, vol. 118, p. 185002.

18. **Melnikov A.V. et al.** Heavy ion beam probing — diagnostics to study potential and turbulence in toroidal plasmas. — Nucl. Fusion, 2017, vol. 57, p. 072004.
19. **Melnikov A.V. et al.** ECRH effect on the electric potential and turbulence in the TJ-II stellarator and T-10 tokamak plasmas. — Plasma Phys. Control. Fusion, 2018, vol. 60, p. 084008.
20. **Svoboda V., Zhekova M., Dimitrova M., Marinova P., Podolnik A., Stockel J.** Operational Domain in hydrogen plasmas on the GOLEM tokamak. — J. of Fusion Energy, 2019, vol. 38, pp. 253—261.
21. **Svoboda V. et al.** Operational Domain in Hydrogen Plasmas on the GOLEM Tokamak. — J. of Fusion Energy, 2019, vol. 38, pp. 253—261.
22. **Svoboda V., Huang B., Mlynar J. et al.** Multi-mode remote participation on the GOLEM tokamak. — Fusion Eng. Des., 2011, vol. 86, pp. 1310—1314.
23. **Hutchinson I.H.** Principles of plasma diagnostics. — New York: Cambridge University Press, 1987. 440 p.
24. **Mirnov S.V.** A probe method for measuring the displacement of the current channel in cylindrical and toroidal discharge vessels. — J. Nucl. Energy. Part C Plasma Phys., 1965, vol. 7, p. 325.
25. **Adámek J. et al.** Diagnostics of magnetized low temperature plasma by ball-pen probe. — Nukleonika, 2012, vol. 57(2), pp. 297—300.
26. **Mácha P.** Měření základních parametrů okrajového plazmatu pomocí kombinované ball-pen a Langmuirovy sondy na tokamaku GOLEM. — Bachelor Thesis.
27. **Valovic M.** Convective losses during current initiation in tokamaks. — Nuclear Fusion, 1987, vol. 27, p. 599.
28. **Lloyd B., Carolan P.G., Warrick C.D.** ECRH-assisted start-up in ITER. — Plasma Phys. Control. Fusion, 1996, vol. 38 (9), p. 1627.
29. **Brotankova J., Dthesis Ph.** http://golem.fjfi.cvut.cz/wiki/Library/GOLEM/PhDthesis/JanaBrotankovaPhDthesis.pdf.
30. **Goldston R.J.** Energy confinement scaling in tokamaks: some implications of recent experiments with ohmic and strong auxiliary heating PPLR. 1984. https://www.osti.gov/servlets/purl/5208115.
31. **Parker R.R., Greenwald M., Luckhardt S.C., Marmar E.S., Porkolab M., Wolfe S.M.** Progress in tokamak research at mit. 1985. https://dspace.mit.edu/bitstream/handle/1721.1/94844/85ja014_full.pdf?sequence=1.
32. **Hillaret J.** https://clck.ru/ScMwn (golem/wiki/scaling.png).
33. **Smith D.E., Powers E.J., Caldwell G.S.** Fast-fourier-transform spectral-analysis techniques as a plasma fluctuation diagnostic tool. — IEEE Trans. on Plasma Sci., 1974, vol. 2 (4), pp. 261—272.
34. **Vershkov V.A., Shelukhin D.A., Soldatov S.V. et al.** Summary of experimental core turbulence characteristics in ohmic and electron cyclotron resonance heated discharges in T-10 tokamak plasmas. — Nucl. Fusion, 2005, vol. 45 (10), S203—S226.
35. **Drabinskiy M.A., Eliseev L.G., Khabanov P.O. et al.** Radial structure of quasi-coherent mode in ohmic plasma of the T-10 tokamak. — J. of Phys.: Conf. Series, 2019, vol. 1383, p. 012004.
36. **Kramer-Flecken A. et al.** Turbulence studies with means of reflectometry at TEXTOR. — Nucl. Fusion, 2004, vol. 44, p. 1143.
37. **Kuznetsov Yu.K., Nascimento I.C., Silva C. et al.** Long-distance correlations in TCABR biasing experiments. — Nucl. Fusion, 2012, vol. 52, p. 063004.
38. **Malaquias A., Henriques R.B., Nedzelsky I.S.** Inversion methods for the measurements of mhd-like density fluctuations by heavy ion beam diagnostic. — J. of Instr., 2015, vol. 10 (09), p. 09024.
39. **Melnikov A.V., Markovic T., Eliseev L.G. et al.** Quasicoherent modes in the COMPASS tokamak. — Plasma Phys. and Control. Fusion, 2015, vol. 57, p. 065006.
40. **Vershkov V.A., Shelukhin D.A., Subbotin G.F. et al.** Density fluctuations as an intrinsic mechanism of pressure profile formation. — Nucl. Fusion, 2015, vol. 55, p. 063014.
41. **Vershkov V.A., Buldakov M.A., Subbotin G.F. et al.** 3D structure of density fluctuations in the T-10 tokamak and new approach for current profile estimation. — Nucl. Fusion, 2019, vol. 59 (6), p. 066021.
42. **Eliseev L., Melnikov A., Perfilov S. et al.** Two point correlation technique for the measurements of poloidal plasma rotation by heavy ion beam probe. — Plasma and Fusion Research, 2012, vol. 7, p. 2402064.
43. **Basu D. et al.** Geodesic acoustic mode (GAM) like oscillations and RMP effect in the STOR-M tokamak. — Nucl. Fusion, 2018, vol. 58. p. 024001.

AUTHORS

Sarancha G.A. NRC “Kurchatov Institute”, pl. Akademika Kurchatova 1, 123182 Moscow, Russia; Moscow Institute of Physics and Technology (National Research University), Institutskiy per. 9, 141700 Dolgoprudnyi, Moscow region, Russia; sarancha.ga@phystech.edu

Drozd A.S. NRC "Kurchatov Institute", pl. Akademika Kurchatova 1, 123182 Moscow, Russia; National Research Nuclear University MEPhI (Moscow Engineering Physics Institute), Kashirskoye shosse 31, 115409 Moscow, Russia; 970107@bk.ru

Emekeev I.A. NRC "Kurchatov Institute", pl. Akademika Kurchatova 1, 123182 Moscow, Russia; Moscow Institute of Physics and Technology (National Research University), Institutskiy per. 9, 141700 Dolgoprudnyi, Moscow region, Russia; emekeev.ia@phystech.edu

Ganin S.A. NRC "Kurchatov Institute", pl. Akademika Kurchatova 1, 123182 Moscow, Russia; National Research Nuclear University MEPhI (Moscow Engineering Physics Institute), Kashirskoye shosse 31, 115409 Moscow, Russia; stas.ganin.97@mail.ru

Kropackova D. Faculty of Nuclear Sciences and Physical Engineering, Czech Technical University in Prague, Brzhekhova 7, 115 19 Prague 1, Czech Republic; DaniKropack@seznam.cz

Kudashev I.S. NRC "Kurchatov Institute", pl. Akademika Kurchatova 1, 123182 Moscow, Russia; National Research Nuclear University MEPhI (Moscow Engineering Physics Institute), Kashirskoye shosse 31, 115409 Moscow, Russia; wave880@gmail.com

Kulagin V.V. NRC "Kurchatov Institute", pl. Akademika Kurchatova 1, 123182 Moscow, Russia; National Research Nuclear University MEPhI (Moscow Engineering Physics Institute), Kashirskoye shosse 31, 115409 Moscow, Russia; kulagin.vladimir.l@yandex.ru

Lauerova M. Faculty of Nuclear Sciences and Physical Engineering, Czech Technical University in Prague, Brzhekhova 7, 115 19 Prague 1, Czech Republic; Gymnasium «Nový PORG», 14200, Pod Krchskim lesem 1300/25, Prague 4, Czech Republic; martina.lauerova@gmail.com

Melnikov A.V. NRC "Kurchatov Institute", pl. Akademika Kurchatova 1, 123182 Moscow, Russia; Moscow Institute of Physics and Technology (National Research University), Institutskiy per. 9, 141700 Dolgoprudnyi, Moscow region, Russia; National Research Nuclear University MEPhI (Moscow Engineering Physics Institute), Kashirskoye shosse 31, 115409 Moscow, Russia; Melnikov_07@yahoo.com

Sergeev N.S. NRC "Kurchatov Institute", pl. Akademika Kurchatova 1, 123182 Moscow, Russia; National Research Nuclear University MEPhI (Moscow Engineering Physics Institute), Kashirskoye shosse 31, 115409 Moscow, Russia; nickbebeskis@gmail.com

Krokhalev O.D. NRC "Kurchatov Institute", pl. Akademika Kurchatova 1, 123182 Moscow, Russia; Moscow Institute of Physics and Technology (National Research University), Institutskiy per. 9, 141700 Dolgoprudnyi, Moscow region, Russia; krohalev.od@phystech.edu

Stockel J. Faculty of Nuclear Sciences and Physical Engineering, Czech Technical University in Prague, Brzhekhova 7, 115 19 Prague 1, Czech Republic;stockel@ipp.cas.cz

Svoboda V. Faculty of Nuclear Sciences and Physical Engineering, Czech Technical University in Prague, Brzhekhova 7, 115 19 Prague 1, Czech Republic; Vojtech.Svoboda@fjfi.cvut.cz

Received 1 August 2021
Revised 28 August 2021
Accepted 28 September 2021
Problems of Atomic Science and Technology
Ser. Thermonuclear Fusion, 2021, vol. 44, issue 4, pp. 92—110